Improving Channel Capacity in the LTE Downlink through Channel Prediction

Francis Gichohi Karuga

A thesis submitted in partial fulfillment for the degree of Master of Science in Telecommunication Engineering in the Jomo Kenyatta University of Agriculture and Technology

2017

DECLARATION

This thesis is my original work and has not been presented for a degree in any other University

Signature: _____ Date: _____

Francis Gichohi Karuga

This thesis has been submitted for examination with our approval as university supervisors.

Signature: _____ Date: _____

Dr. Edward Ndungu,

JKUAT, Kenya

Signature: _____ Date: _____

Dr. Kibet Langat,

JKUAT, Kenya

DEDICATION

I dedicate this work to my first and greatest teacher, my late mum Marjorie Wangari Gichohi. For inspiring in me the love of knowledge, for her sacrifices for her family throughout her life and for her unceasing love.

Farewell MUM.

ACKNOWLEDGEMENTS

I would also like to thank my supervisors Dr. Edward Ndungu and Dr. Kibet Langat for their support and guidance throughout my research work. Their outstanding expertise and tireless advice greatly improved the technical content and the presentation of this thesis.

I would also like to acknowledge the financial support of the Kenya Education Network (KENET) for their sponsorship to the IEEE AFRICON 2015 conference in Addis Ababa.

Finally, I would like to thank my family Wanjiru, Karuga and Wangari for their support and understanding throughout the period of this work.

TABLE OF CONTENTS

LIST OF FIGURES

LIST OF TABLES

LIST OF ACRONYMS

3D-MMSE	Three Dimension Minimum Mean Square Error.
3G	Third Generation.
3GPP	Third Generation Partnership Project.
4G	Fourth Generation.
A3D-MMSE	Approximate Three Dimension Minimum Mean Square Error.
ADS	Azimuth Delay Spread.
AMMSE	Approximate Minimum Mean Square Error.
AOA	Angle of Arrival.
AOD	Angle of Departure.
AR	Autoregressive.
AS	Azimuth Spread.
AWGN	Additional Gaussian White Noise.
BLER	Block Error Rate.
BS	Base Station.
CIR	Channel Impulse Response.
CP	Cyclic Prefix.
CQI	Channel Quality Indicator.
CSI	Channel State Information.
CSR	Cell Specific Reference.
DLSCH	Downlink Shared Channel.
DOA	Direction of Arrival.
E-UTRAN	Evolved UMTS Terrestrial Radio Access Network.
EESM	Exponential Effective SINR Mapping.
eNB	Evolved Node B.
EPC	Evolved Packet Core.

ESM Effective SINR Mapping.

ESPRIT Estimation of Signal Parameters via Rotational Invariance Techniques.

FIR Finite Impulse Response.

FT Fourier Transform.

ICI Intercarrier Interference.

IDFT Inverse Discrete Fourier Transform.

IFFT Inverse Fast Fourier Transform.

ISI Inter-Symbol Interference.

LS Least Squares.

LTE Long Term Evolution.

LTE-A Long Term Evolution - Advanced.

MIESM Mutual Information Effective SINR Mapping.

MIMO Multiple Input Multiple Output.

MMSE Minimum Mean Square Error.

MSE Mean Square Error.

MT Mobile Terminal.

MUSIC MUltiple Signal Classification.

NLMS Normalised Linear Mean Square.

OFDM Orthogonal Frequency Division Multiplexing.

OFDMA Orthogonal Frequency Division Multiple Access.

PADS Power Azimuth Delay Spread.

PAPR Peak to Average Power Ratio.

PAS Power Azimuth Spectrum.

PDLSCH Physical Downlink Shared Channel.

PDS Power Delay Spectrum.

PMI Precoding Matrix Indicator.

QAM Quadrature Amplitude Modulation.

QPSK	Quadrature Phase Shift Keying.
RB	Resource Block.
RI	Rank Indicator.
RLS	Recursive Least Squares.
SCM	Spatial Channel Model.
SCME	Spatial Channel Model Extended.
SFBC	Space Frequency Block Coding.
SINR	Signal to Interference Noise Ratio.
SISO	Single Input Single Output.
SNR	Signal to Noise Ratio.
STBC	Space Time Block Coding.
SVD	Singular Value Decomposition.
UE	User Equipment.
UMTS	Universal Mobile Telecommunication System.
WCDMA	Wideband Code Division Multiple Access.
WINNER	Wireless World Initiative New Radio.

LIST OF SYMBOLS

Symbols

$(\cdot)^T$	Transpose of Matrix
$\mathbb{C}^{N\times M}$	The set of complex-valued $N \times M$ matrices
$\mathbb{E}\{X\}$	Expectation of X
$\mathbf{H}$	bold upper case letters denote matrices
$\mathbf{h}$	bold lower case letters denote vectors
$\mathbf{I}_N$	The $N \times N$ identity matrix
$\mathbf{O}_N$	The $N \times N$ matrix of only zeros
$\mathbf{R_{hh}}$	covariance/correlation matrix of $\mathbf{h}$
$\mathbf{X} \otimes \mathbf{Y}$	Kronecker Product of two matrices $\mathbf{X}$ and $\mathbf{Y}$
$\mathbf{X}^*$	Conjugate of each element of Matrix $\mathbf{X}$
$\mathbf{X}^{-1}$	Inverse of matrix $\mathbf{X}$
$\mathbf{X}^H$	Hermitian Transpose of Matrix $\mathbf{X}$
$\mathbf{X}^T$	Transpose of Matrix $\mathbf{X}$
$\|\cdot\|$	Euclidian Norm
$\|\cdot\|_F$	Frobenius norm
$O(\cdot)$	The Big **O** notation
$tr(\cdot)$	Trace of Matrix
$vec(\mathbf{X})$	The vector obtained by stacking the columns of $\mathbf{X}$

ABSTRACT

Link adaptation, multiuser resource scheduling and adaptive MIMO precoding are implemented in the Long Term Evolution (LTE) downlink in order to improve spectral efficiency and enhance effective utilization of the available radio resources. These processes require the transmitter to have an accurate knowledge of the channel state information (CSI). This is typically provided via feedback from the receiver. Due to processing and feedback delays, the CSI used at the transmitter is outdated leading to performance degradation causing a decrease in the overall system capacity.

Channel prediction is an important technique that can be used to mitigate the system degradation that arises as a result of the inevitable feedback delay. The minimum mean square error (MMSE) based algorithms have been proven to have high performance in channel estimation and prediction. However this superior performance is accompanied by a high computational complexity due to the matrix inversion required as well as the large size of the channel matrix.

In this thesis, the problem of channel aging on the LTE downlink is discussed. After a review of the LTE architecture along with its MIMO-OFDM radio interface, an overview of transmissions through a wireless fading channel is presented. A system model for block fading channels is then presented and a MMSE channel prediction method is derived. A reduced complexity approximate MMSE channel (AMMSE) prediction algorithm is then proposed to reduce the high computational complexity inherent in the MMSE method. The complexity reduction is achieved through reduction of the size of the channel matrix as well as approximating the matrix inversion through iteration. Evaluation of the proposed approximate MMSE algorithm

indicates that the mean square error can be reduced by up to 13 dB for feedback delays of 0 – 15 ms which translates to an improvement of 22% in the average throughput for slow fading channels.

Fast fading channels are characterized by high Doppler spread and are dispersive in both time and frequency. At high Doppler spread, the effects of channel aging become more pronounced and the channel capacity decreases rapidly without prediction. The block fading model which is flat fading and only utilizes the temporal correlations is inadequate for fast fading channels. A novel three dimensional minimum mean square error (3D-MMSE) channel prediction algorithm which utilizes the time, frequency and spatial correlations is developed for the fast fading scenario. The performance of the proposed algorithm in doubly dispersive channels is studied and analyzed. The results indicate that the proposed 3D-MMSE prediction technique provides 17.4 % enhancement in average throughput for feedback delays of 0 – 10 ms compared with the scenario without prediction in fast fading channels. A reduced complexity approximate 3D-MMSE (A3D-MMSE) algorithm is then proposed to reduce the high computational complexity inherent in the 3D-MMSE method. The approximate method operates through a three-step algorithm which first exploits temporal correlations, followed by separate smoothing filters to exploit the frequency and spatial correlations. A comparative analysis indicates that the proposed approximate 3D-MMSE algorithm provides 89 % reduction in complexity compared to the 3D-MMSE algorithm. The results show that an increase in the Doppler spread above 200 Hz leads to decrease in the temporal correlations and this makes the channel prediction to become increasingly inaccurate.

CHAPTER ONE

INTRODUCTION

1.1 BACKGROUND

Consider a scenario in which two people each with a mobile device are moving in an urban environment while communicating. The mobile devices which in LTE are referred to as user equipment (UE) receive a signal from a Base Station (BS) through a wireless radio channel. The transmitted signal typically bounces off the ground, nearby buildings, vehicles and trees before eventually arriving at the User Equipment (UE). The signal which arrives at the UE will be a composite made from the addition of components which have traveled through many different paths. These multiple signal components will interfere with each other and as a result the signal received will have a lot of variations in its strength. Peaks in the signal will occur due to constructive interference while troughs will occur due to destructive interference. This phenomenon is known as fading and its a feature of all wireless systems [1].

All wireless communication systems incorporate multiple strategies for combating the effects of fading. One of these strategies is the dynamic allocation of radio resources in which the BS transmits to the UE with the best channel quality. This is called channel aware scheduling and it has the effect of maximizing the efficiency in the utilization of shared radio resources. With dynamic scheduling, the average quality of reception for each UE is higher than if the resource is shared statically using time slot scheduling [2].

Dynamic scheduling requires the BS to know the channel quality at each UE. This is usually accomplished by having the UE measure the signal strength and send back a report to the BS. A critical problem with this technique is that there is an inevitable delay between the instant of time the UE performs the signal strength measurement to the time the BS performs dynamic scheduling. During this delay interval, it is possible for a UE to have moved from a spot with high signal strength (peak) to a spot with low

signal strength (trough). This problem is especially severe if the users are traveling at high speed e.g. in a vehicle. This issue forms the main motivation for channel prediction, in that the user equipment should report back to the base station the channel state a time period in future and not the current channel state [3, 4].

1.2 A BRIEF OVERVIEW OF CHANNEL PREDICTION

There are two main approaches in linear prediction of a time series. The correlation based sub-sampled direct Finite Impulse Response (FIR) predictor and the model-based predictor, using Autoregressive (AR) models for the dynamics of the time series. As the FIR-predictor also offers a robust low complexity predictor that can fully exploit the correlation in the signal over the lags it uses, it is a natural choice for prediction of the taps of a mobile radio channel. The optimal linear FIR-predictor using past noisy observations to predict a signal is given by the Wiener-Hopf equations [5]. Consider a scenario where a BS transmits a signal at discrete times to a UE. At time n the signal transmitted is denoted as x_n. The received signal can be modeled in time as:

$$y_n = h_n * x_n + z_n \tag{1.1}$$

where h_n is the magnitude of the channel envelope and z_n is the additive noise. Channel prediction can be used to estimate the future values of the channel several steps ahead by using the current and past values $h_n, h_{n-1}, h_{n-2}, ..., h_{n-M}$ [4].

1.3 PROBLEM STATEMENT

The Third Generation Partnership Project (3GPP) Long Term Evolution (LTE) system requires accurate Channel State Information (CSI) to perform downlink functions such as scheduling, precoding and link adaptation at the BS and coherent detection at the UE. The CSI is obtained through feedback from the UE to the BS. There is a time

delay between the instant of channel estimation and the application of the feedback parameters at the transmitter. During this delay interval, the channel state will have changed, a phenomenon known as *channel aging*.

Channel aging creates a situation in which the BS uses incorrect data to perform the downlink functions and can cause severe performance degradation. This thesis addresses the problem of inaccurate CSI caused by channel aging and proposes a solution through channel prediction.

1.4 OBJECTIVES

The main objective is to improve the throughput of the LTE downlink through accurate channel prediction. The specific objectives are:

1. Perform a comparative analysis of practical channel predictors for realistic channel models and delays.

2. Analyze the effects of Doppler spread on the performance of linear channel prediction algorithms.

3. Develop a Minimum Mean Square Error (MMSE) prediction algorithm that offers improvement in channel capacity at high Doppler spread values.

4. Reduce the complexity of the developed prediction algorithm.

1.5 OUTLINE OF THE THESIS

This thesis document is structured as follows:

- **Chapter 2** describes the structure of the lte downlink with emphasis on MIMO technology.

- **Chapter 3** discusses the methodology used for channel prediction in block and fast fading channels.

- **Chapter 4** lays out the scenario of simulation for this research work and analyzes the results obtained from the simulations.
- **Chapter 5** presents a summary of the conclusions drawn from the research and looks ahead to further challenges.

CHAPTER TWO

LITERATURE REVIEW

2.1 INTRODUCTION

The focus of this chapter is to present an overview of the LTE downlink with emphasis on radio resources. The details of downlink processing functions which include multi-antenna systems, adaptive modulation and coding and channel aware link adaptation will be presented. The role of CSI in the downlink processes is explained as well as aspects of CSI acquisition. Finally, the role of channel prediction within the downlink processing protocols is discussed.

2.2 ORTHOGONAL FREQUENCY DIVISION MULTIPLEXING

OFDM, the transmission technique used in LTE is a multi-carrier scheme in which a large number of closely spaced sub-carriers are used to transmit data. OFDM has several features that make it suitable for wireless communication systems such as; its high spectral efficiency, robustness to fading, low complexity implementation especially with the advent of digital signal processors and support for advanced features such as MIMO techniques [6].

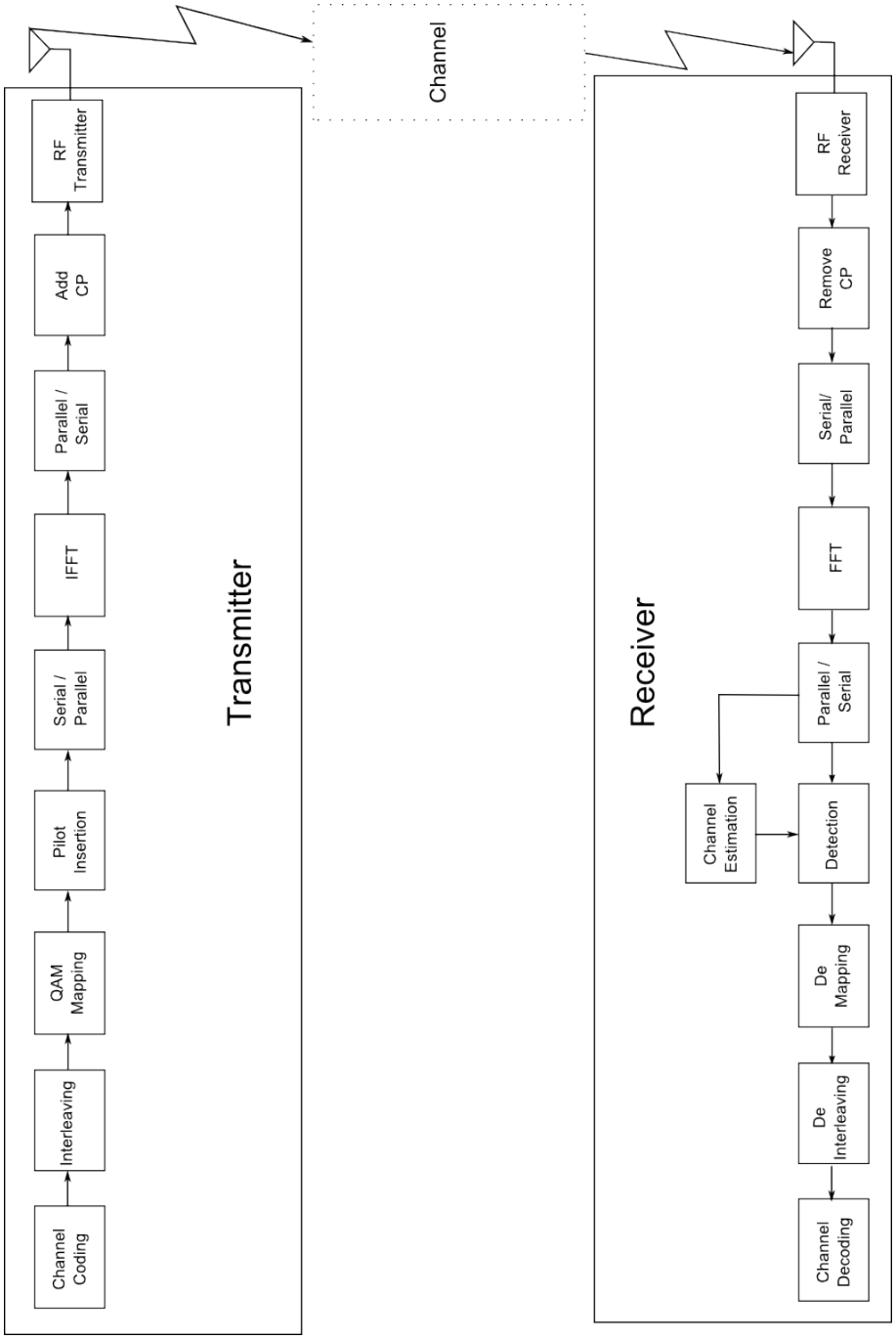

Fig. 2.1 OFDM Block Diagram

Figure 2.1 shows a typical block diagram for an OFDM transmitter. A serial -parallel converter converts a single high data rate stream into multiple low data rate sequences. These data streams are then independently modulated using Quadrature Phase Shift Keying (QPSK) or Quadrature Amplitude Modulation (QAM) modulation

techniques on different sub-carriers. The resulting vector is then applied as the input to an N-point Inverse Discrete Fourier Transform (IDFT) which produces a set of N complex time domain samples belonging to one OFDM symbol.

At the beginning of each OFDM symbol, a cyclic prefix (CP) is inserted to create a guard period between symbols. This is done to eliminate the Inter-Symbol Interference (ISI) caused by multipath fading.

2.3 OFDM BASEBAND SIGNAL

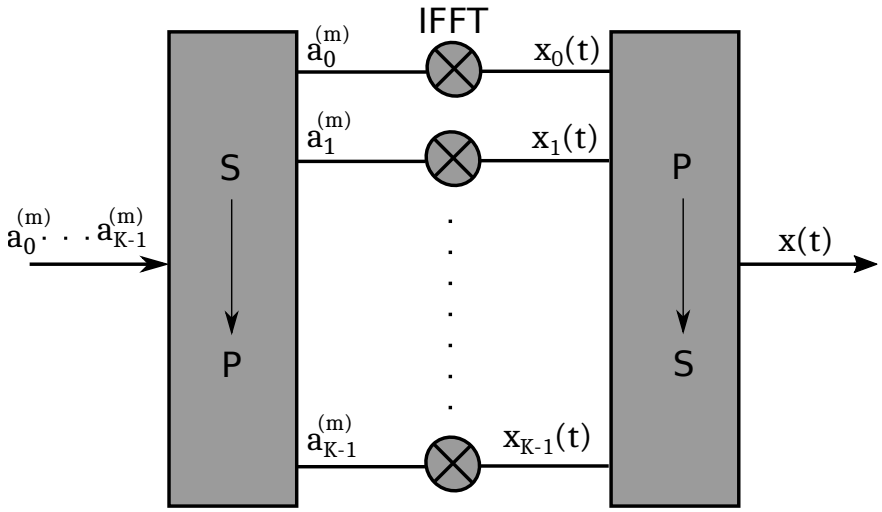

Fig. 2.2 OFDM Baseband Signal

A simplified OFDM modulator is illustrated in Figure 2.2, where K modulators each corresponding to a subcarrier are deployed. The subcarriers have a spacing of $\Delta t = {}^{1}/_{T_s}$ where T_s is the per-subcarrier modulation-symbol time [7]. The baseband OFDM signal during the m^{th} OFDM symbol time $mT_s < t < (m+1)T_s$ is expressed as:

$$x(t) = \sum_{k=0}^{K-1} x_k(t) = \sum_{k=0}^{K-1} a_k^{(m)} e^{j2\pi k\Delta f t} \tag{2.1}$$

where $x_k(t)$ is the k^{th} subcarrier, Δf is the subcarrier bandwidth and $a_k^{(m)}$ is the modulation symbol applied to the k^{th} subcarrier during the m^{th} OFDM symbol. The term orthogonal means that any two subcarriers during the m^{th} OFDM symbol have a relationship expressed as:

$$\int_{mT_s}^{(m+1)T_s} x_{k_1}(t)x_{k_2}^*(t)dt = 0 \tag{2.2}$$

Consider a discrete time OFDM where the sampling rate $f_s = N\Delta f$ and $N > K$. The OFDM signal of (2.1) can be written as:

$$\begin{aligned} x(nT_s) &= \sum_{k=0}^{K-1} a_k e^{j2\pi k\Delta f n T_s} \\ &= \sum_{k=0}^{K-1} a_k e^{j2\pi kn/N} \\ &= \sum_{k=0}^{N-1} a_k e^{j2\pi kn/N} \end{aligned} \tag{2.3}$$

Equation (2.3) shows that the sampled OFDM signal is the N-point IDFT of the modulation symbols $a_0, a_1, \cdots, a_{K-1}$ extended with zeros to length N. By choosing a value for N that is an integer multiple of 2, then OFDM can be implemented by means of the efficient Inverse Fast Fourier Transform (IFFT) algorithms.

Time dispersion in the radio channel can lead to to a loss of orthogonality between adjacent subcarriers as a result of symbol signal overlap. To mitigate against this problem, Cyclic Prefix (CP) insertion is implemented in OFDM. This consists of copying the last part of the OFDM symbol and inserting it the start of the symbol. This in practice implies that the last N_{cp} samples of the IFFT block of length N are copied and inserted at the start of the symbol. At the receiver side the CP is discarded before demodulation and subsequent receiver processing.

The n^{th} output of the IFFT block in Figure 2.1 is expressed as:

$$x_n = \frac{1}{\sqrt{N}} \sum_{k=0}^{N-1} X_k e^{j2\pi nk/N} \tag{2.4}$$

Assuming the number of paths between the transmitter and receiver is L, the output of the channel is given by:

$$y_n = \sum_{l=0}^{L-1} h_{n,l} x_{n,l} + z_n \tag{2.5}$$

where $h_{n,l}$ is the Channel Impulse Response (CIR) of the l^{th} path and z_n is the Additional Gaussian White Noise (AWGN). From 2.4, the channel output can be expressed as:

$$\begin{aligned} y_n &= \left(\frac{1}{\sqrt{N}} \sum_{l=0}^{L-1} h_{n,l} \sum_{k=0}^{N-1} X_k e^{j2\pi(n-l)k/N} \right) + z_n \\ &= \left(\frac{1}{\sqrt{N}} \sum_{k=0}^{N-1} X_k e^{j2\pi nk/N} \sum_{l=0}^{L-1} h_{n,l} e^{j2\pi lk/N} \right) + z_n \end{aligned} \tag{2.6}$$

The Fourier Transform (FT) of the CIR, denoted as H_n is given by:

$$H_n = \sum_{l=0}^{L-1} e^{-j2\pi lk/N} \tag{2.7}$$

The channel output thus becomes:

$$y_n = \left(\frac{1}{\sqrt{N}} \sum_{k=0}^{N-1} X_k H_n^{(k)} e^{j2\pi nk/N} \right) + z_n \tag{2.8}$$

The modulated symbol at the receiver is given by:

$$Y_k = \frac{1}{\sqrt{N}} \sum_{n=0}^{N-1} y_n e^{-j2\pi nk/N} \tag{2.9}$$

$$
\begin{aligned}
Y_k &= \frac{1}{\sqrt{N}} \sum_{n=0}^{N-1} \left(\frac{1}{\sqrt{N}} \sum_{m=0}^{N-1} X_m H_n^{(m)} e^{j2\pi nm/N} + z_n \right)^{-j2\pi nk/N} \\
&= \frac{1}{N} \sum_{k=0}^{N-1} X_k \sum_{n=0}^{N-1} H_n^{(k)} e^{-j2\pi(k-m)n/N} + \frac{1}{\sqrt{N}} \sum_{n=0}^{N-1} z_n e^{-j2\pi nk/N} \\
&= \left[\frac{1}{N} \sum_{n=0}^{N-1} H_n^{(k)} \right] X_k + \left[\frac{1}{N} \sum_{k=0, k\neq m}^{N-1} X_k \sum_{n=0}^{N-1} H_n^{(m)} e^{-j2\pi(k-m)n/N} \right] + Z_k \\
&= H_k X_k + \beta_k + Z_k
\end{aligned}
\tag{2.10}
$$

where,

$$
H_k = \frac{1}{N} \sum_{n=0}^{N-1} H_n^{(k)} \tag{2.11}
$$

$$
\beta_k = \frac{1}{N} \sum_{k=0, k\neq m}^{N-1} X_k \sum_{n=0}^{N-1} H_n^{(m)} e^{-j2\pi(k-m)n/N} \tag{2.12}
$$

$$
Z_k = \frac{1}{\sqrt{N}} \sum_{n=0}^{N-1} z_n e^{-j2\pi nk/N} \tag{2.13}
$$

H_k is the frequency response of the CIR, Z_k is the Fourier Transform of the AWGN and β_k is the Intercarrier Interference (ICI) caused by the time varying nature of the channel. In a slow fading channel the Doppler frequency is small and the ICI is approximately zero and can be ignored. On the contrary, in fast fading channels with a high Doppler spread, the effect of the ICI cannot be ignored and it leads to a reduction in the power of the desired signal.

OFDMA is a multi-access technique that is based on OFDM. It allows multiple users to access available radio resources at the same time thus permitting the sharing of the system bandwidth. In a MIMO based OFDMA system the shared resources are frequency in the form of subcarriers, time in the form of time slots and the antenna ports. Based on feedback parameters received from the Mobile Terminal (MT), adaptive

resource scheduling is performed at the BS to equitably allocate these resources. In LTE, time-frequency entities known as Resource Block (RB) are shared among users as illustrated in Figure 2.3.

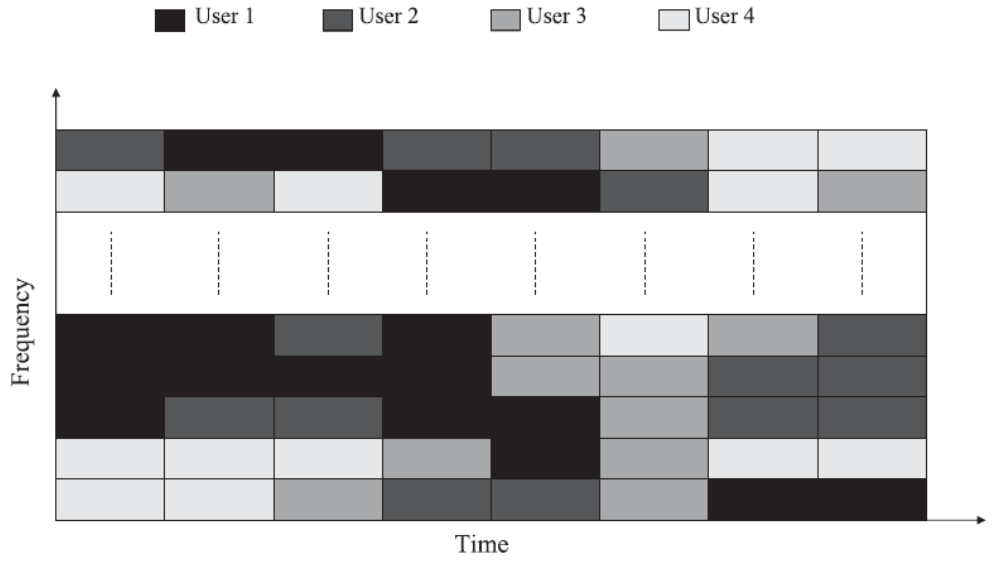

Fig. 2.3 OFDMA Resource Scheduling

2.4 AN OVERVIEW OF LONG TERM EVOLUTION

The Long Term Evolution (LTE) system is a mobile standard that was developed through a collaboration of several international telecommunications standards bodies collectively known as the 3GPP and it is known in full as 3GPP LTE. It evolved from theUniversal Mobile Telecommunication System (UMTS) which is the most dominant Third Generation (3G) system in the world. The main difference between UMTS and LTE was the change in the radio interface from Wideband Code Division Multiple Access (WCDMA) to OFDMA and the move to a flat core network architecture. LTE is a mobile communication standard first standardized in LTE Release 8 in 2008. Long Term Evolution - Advanced (LTE-A) was the first Fourth Generation (4G) mobile system based on the criterion set by the 3GPP. According to the 3GPP, the creation of the LTE standard has been motivated by among others [8]:

- Creation of new services for mobile devices such as video calls and online gaming which require higher data rates.
- Need to have a unified system for both voice and data that is packet based.
- Exponential growth in data traffic meant networks were increasingly becoming congested as a result in capacity limits.
- Low complexity
- The need to avoid unnecessary fragmentation of technologies for paired and unpaired band operation.

2.5 HIGH LEVEL ARCHITECTURE

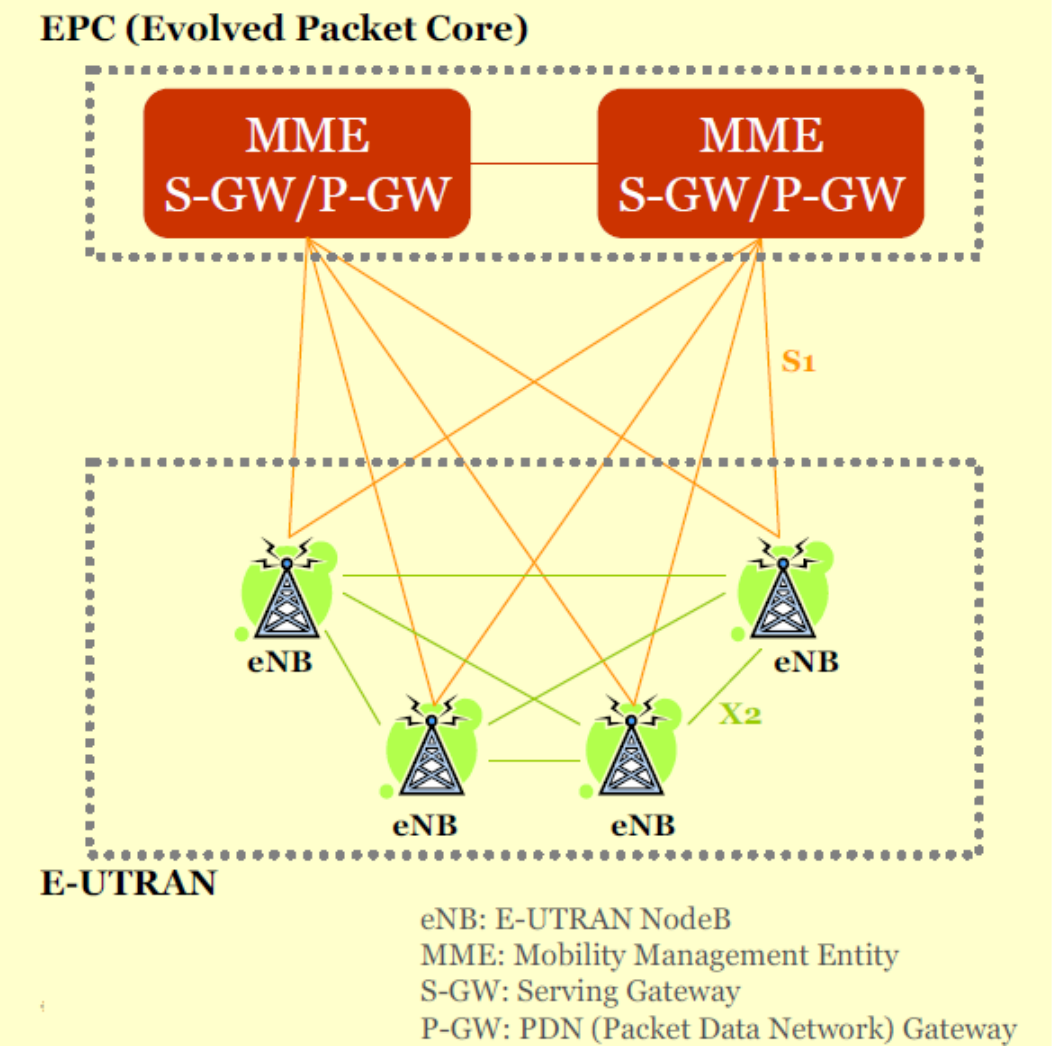

Fig. 2.4 LTE High Level Architecture

At a high level, the LTE network consists of three main components, the MT, the Evolved UMTS Terrestrial Radio Access Network (E-UTRAN) and the Evolved Packet Core (EPC) [9] as shown in Fig 2.4. The E-UTRAN handles communications between the mobile device and the core network and contains a single component, the Evolved Node B (eNB). This is a BS that controls the mobiles in a cell. Each eNB is connected to the EPC via an S1 interface which can be a wireless or fixed connection.

2.6 LTE DOWNLINK

Table 2.1 LTE Downlink Parameters

Transmission BW (MHZ)	1.25	2.5	5	10	15	20
Subcarrier bandwidth (kHz)	5	5	5	5	5	5
Subframe Duration (ms)	1	1	1	1	1	1
Number of RBs	6	12	25	50	75	100
FFT Size	128	256	512	1024	1536	2048
Sampling Frequency (MHz)	1.92	3.84	7.68	15.36	23.04	30.72

The LTE downlink is designed to accommodate bandwidths from 1.25 MHz to 25 MHz. The subcarrier spacing is 15 KHz with a subframe of 1 ms. Depending on the delay spread, a short or long CP is appended to the symbol. The specifications are summarized in Table 2.1 [10].

2.6.1 AIR INTERFACE

The LTE downlink air interface is based on Orthogonal Frequency Division Multiple Access (OFDMA) which shares the available radio resource to multiple users according to a scheduling algorithm [11]. This resource is organized in a time frequency grid as illustrated in Figure 2.5.

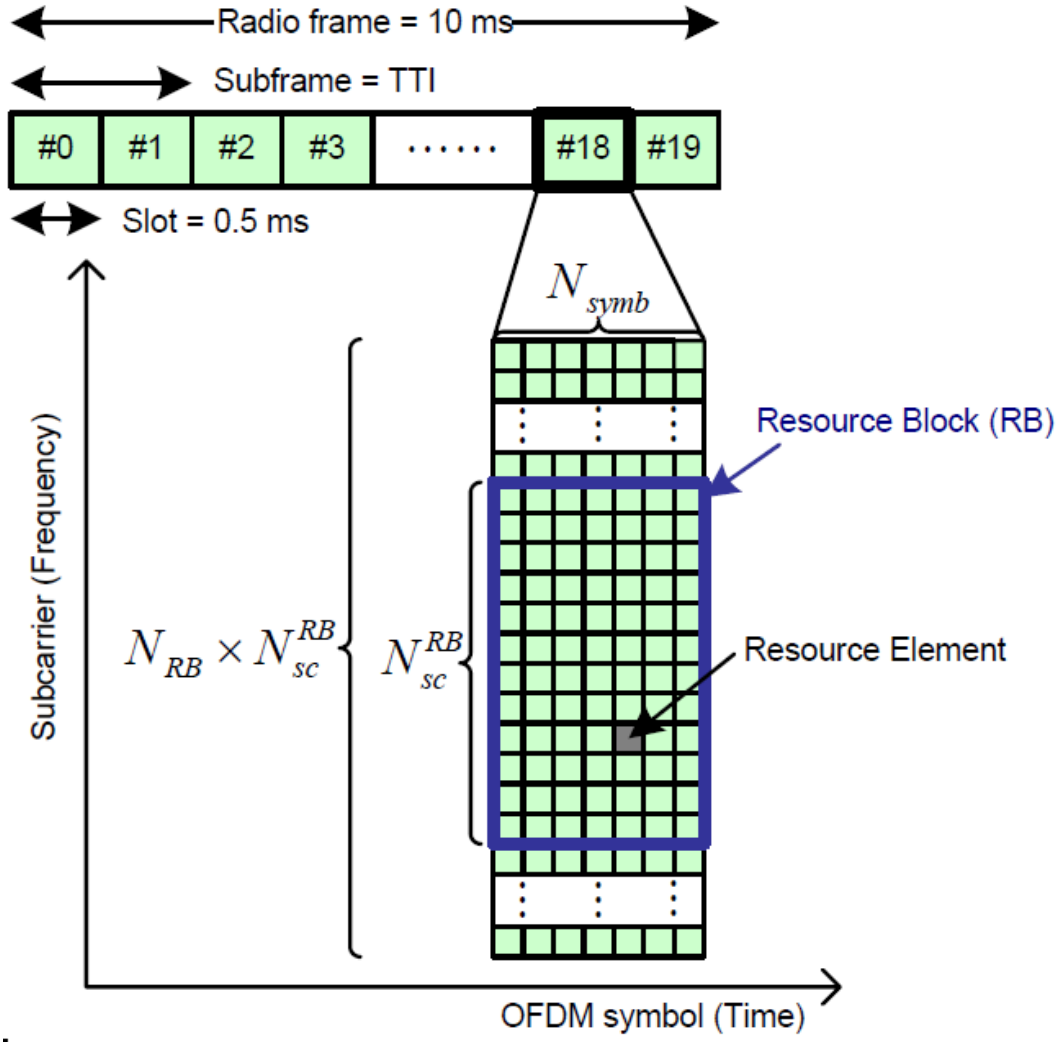

Fig. 2.5 Time Frequency Grid of LTE Downlink.

The radio resource of LTE is organized as follows: the largest unit of time if the radio frame of duration 10 ms, the radio frame is subdivided into ten subframes of 1 ms each which in turn are split into two time slots of 0.5 ms. Each time slot comprises of seven OFDM symbols. In frequency, the smallest unit is called a Resource Element (RE). One RE is comprised of one subcarrier in a single time slot. A group of 12 subcarriers with each having a bandwidth of 15 kHz in a duration of a single time slot is called a Resource Block (RB) [9].

2.6.2 CELL SPECIFIC REFERENCE SIGNALS

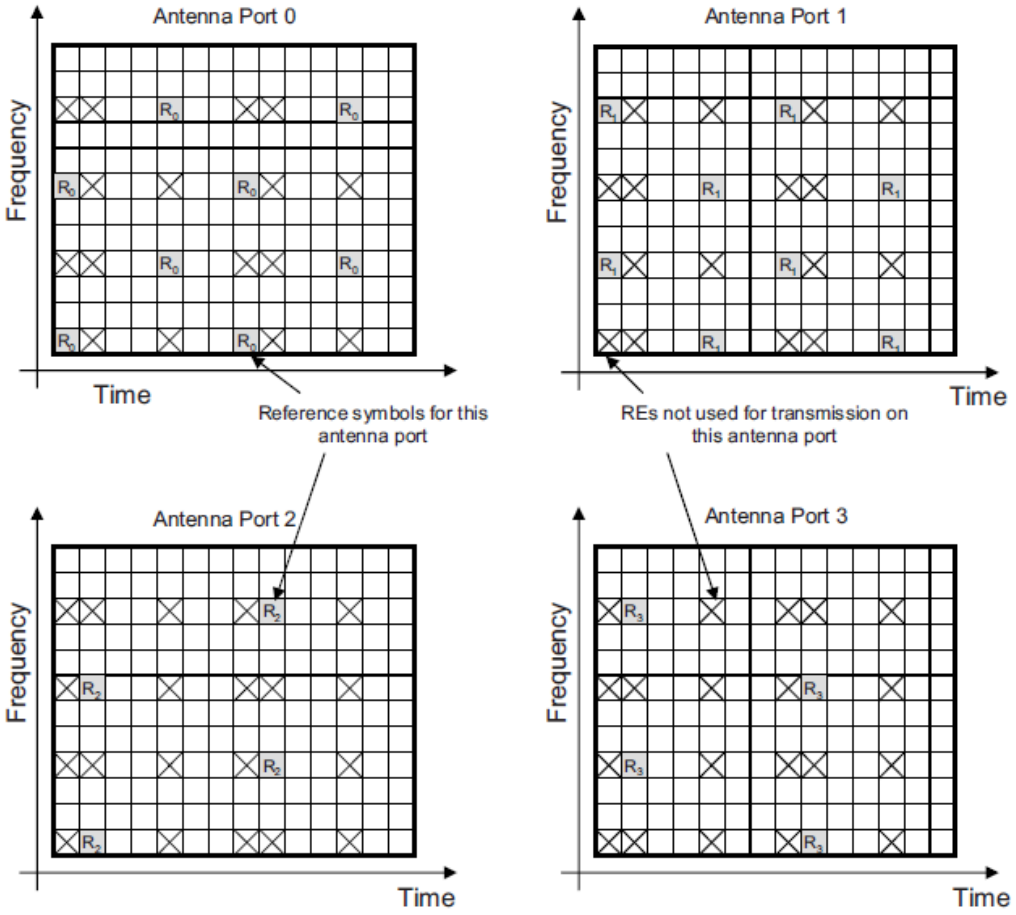

Fig. 2.6 CSR signals for a 4 transmitter system

Fading in wireless radio channels causes ICI in the received signal. Signal detection and equalization at the receiver are used in order to reverse the distortion caused by the channel. When the detection technique utilizes channel knowledge, it is referred to as coherent detection and this requires accurate channel estimation to be performed at the receiver. A common and effective way to perform the required estimation is by inserting predefined signals at the transmitter known as CSR signals or pilots [12]. The position of these pilots in the time-frequency grid depend on the number of transmitter antennas. Figure 2.6 depicts the pilot structure for a system with 4 transmitter antennas.

Within the RB for the first and second antennas there are 4 pilot symbols while the third and fourth antennas have only two pilots in order to reduce the overhead. The pilots are modulated using QPSK with the intention of achieving a low Peak to Average Power Ratio (PAPR). The pilot signal can be expressed as [13]:

$$r_{l,n_s}(m) = \frac{1}{\sqrt{2}}\left[1-2c(2m)\right] + \frac{j}{\sqrt{2}}\left[1-2c(2m+1)\right] \tag{2.14}$$

where m is the index of the CSR, n_s is the slot number within a frame and l is the symbol number within a slot.

2.7 MULTIPLE INPUT MULTIPLE OUTPUT

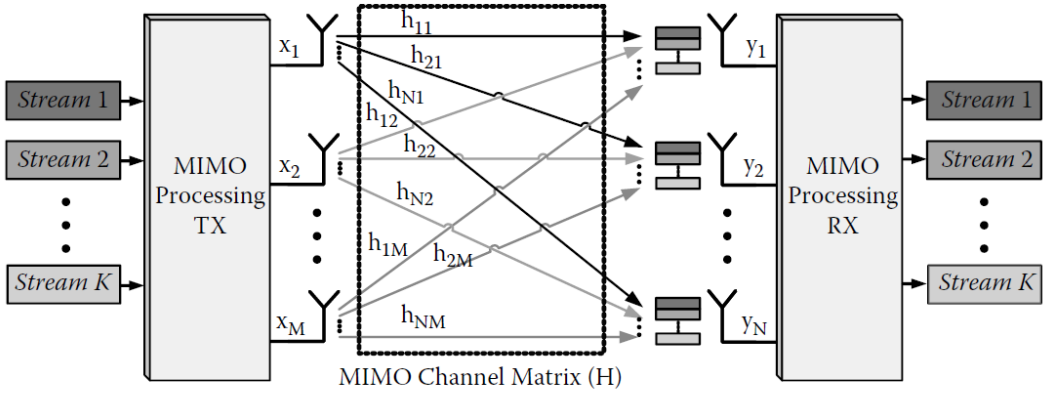

Fig. 2.7 MIMO Transmitter

Multiple Input Multiple Output systems are wireless communication networks that employ multiple antennas both at the transmitter and receiver. Figure 2.7 illustrates a 4x4 MIMO configuration where multiple antennas interconnect the transmitter to the receiver through a channel. At each receiver antenna, the relationship between the received symbol and the transmitted symbol is expressed through a system of linear equations, usually represented in matrix-vector format as $\mathbf{y} = \mathbf{Hx}$ where $\mathbf{H}$ is the channel matrix. In LTE-MIMO based systems, data sent through each transmit-receive antenna

pair is called a layer. Under ideal conditions, MIMO technology has the potential to scale the system throughput linearly as a function of the number of layers. For optimal MIMO performance, a rich scattering environment which ensures a full rank channel matrix is necessary [14]. Since wireless channel conditions as well as UE capabilities can vary to a large degree, it is imperative that MIMO systems are able to adapt to these variations. LTE supports multiple MIMO transmission modes which can be changed dynamically at run time in order to adapt to the current channel conditions. Table 2.2 illustrates these MIMO types.

Table 2.2 Types of MIMO

Transmission Mode	**Downlink Transmission Scheme**
Mode 1	Single Antenna Port
Mode 2	Transmit Diversity
Mode 3	Open-Loop Spatial Multiplexing
Mode 4	Closed-Loop Spatial Multiplexing
Mode 5	Multi-User MIMO
Mode 6	Closed-Loop Rank-1 Spatial Multiplexing

Modes 2, 3, 4, and 6 are Single-User MIMO (SU-MIMO) modes in which a transmitter equipped with multiple antennas sends to a UE which has one or more receive antennas. Dynamic selection of the most effective SU-MIMO mode requires an accurate of knowledge of the channel state by the UE[15].

2.7.1 TRANSMIT DIVERSITY

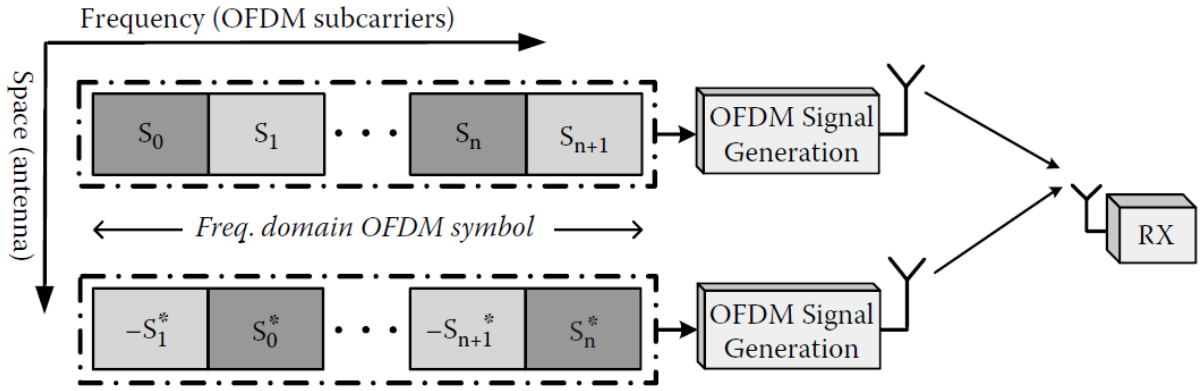

Fig. 2.8 Space Frequency Block Coding

Transmit diversity is a multiple antenna technique which provides an improvement in the signal to noise ratio (SNR) of the received signal through antenna redundancy. Multiple antennas at the transmitter are used to send the same signal. These two signals follow different paths to the receiver and then the multiple components are combined at the receiver. The basic principle being to provide the receiver with multiple copies of the transmitted signal in an attempt to combat the effects of fading. This technique is typically implemented under low Signal to Noise Ratio (SNR) conditions usually when the channel state is poor. Transmit diversity belongs to a class of techniques known as Space Time Block Coding (STBC) although LTE implements the related technique of Space Frequency Block Coding (SFBC) [16]. In SFBC, the Alamouti scheme is applied in the frequency domain [17]. As illustrated in Figure 2.8, the SFBC is performed on complex OFDM symbols. These symbols are mapped directly on the subcarriers of the first antenna. For the second antenna, the mapping is reversely ordered, complex conjugated and sign reversed [18].

2.7.2 SPATIAL MULTIPLEXING

Spatial Multiplexing operates by subdividing a high data rate signal into several lower rate signals and then sending each via different transmit-receive antennas or layers. This however is accompanied by the risk of loss of redundancy in the transmitted signal thereby making spatial multiplexing susceptible to rank reduction in the channel matrix. To combat rank reduction, LTE employs the techniques of adaptive precoding and rank estimation so that it becomes more sturdy in the presence of channel imperfections [19].

The benefits of MIMO depend largely on the availability of channel with a high degree of scattering, which enables the creation of multiple independent paths between the transmitter and receiver. In typical wireless environments, such a channel is not always available.

RANK REDUCTION

Rank reduction in MIMO system refers to the decrease in the number of independent paths between the transmitter and receiver due to limited amount of scatterers in the radio propagation environment.

$$\mathbf{Y}_{n,k} = \begin{bmatrix} H_{n,1,1,k} & . & . & . & H_{n,1,N_T,k} \\ . & & . & . & . \\ H_{n,N_R,1,k} & . & . & . & H_{n,N_R,N_T,k} \end{bmatrix} \begin{bmatrix} x_{n,1,k} \\ . \\ x_{n,N_T,k} \end{bmatrix} + \begin{bmatrix} z_{n,1,k} \\ . \\ z_{n,N_T,k} \end{bmatrix} \tag{2.15}$$

Consider a 4x4 MIMO system represented by (2.15). If the paths between the transmit and receive antennas are similar, then some of the rows and/or columns of the channel matrix can become identical. This reduces the number of linearly independent equations i.e. the matrix rank from four to three. The MIMO equation represented by the resulting channel matrix cannot then be uniquely solved.

PRECODING

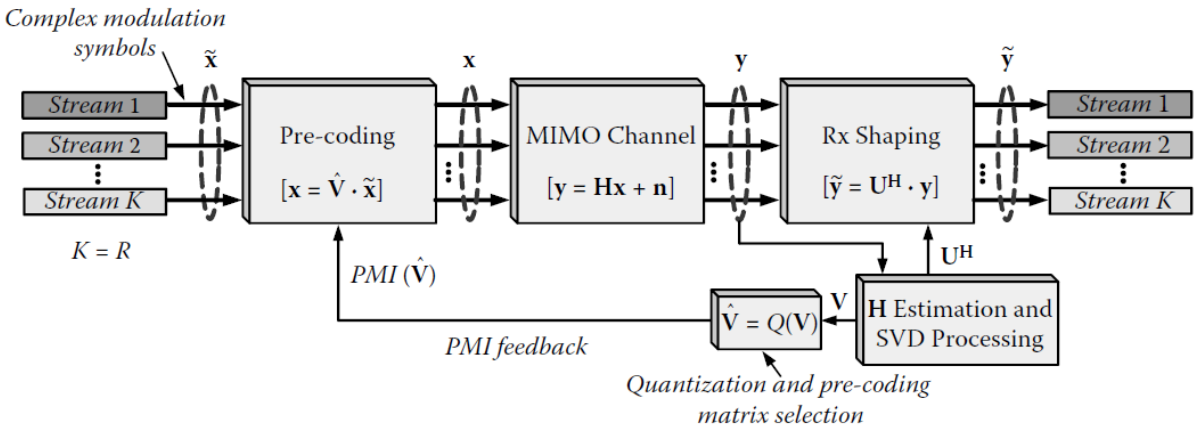

Fig. 2.9 Precoding Based Spatial Multiplexing

The number of independent spatial channels is limited to the rank of the channel matrix. If the CSI is available precoding can be performed to prevent the occurrence of rank reduction and maintain the independence of the spatial channels. Precoding can be viewed as a technique to produce a diagonal channel matrix [12]. It is based on the Singular Value Decomposition (SVD) of the MIMO channel expressed as:

$$\mathbf{H} = \mathbf{U}\mathbf{D}\mathbf{V}^{H} \tag{2.16}$$

where **U** and **V** are matrices whose columns are orthonormal and **D** is a diagonal matrix. Through the application of the precoding matrix **V** before transmission and the shaping matrix $\mathbf{U}^{H}$ after reception, the diagonalization of **D** is achieved. The eigenvalues of $\mathbf{H}\mathbf{H}^{H}$ determine the capacity gain for each spatial channel [18]. The SVD process is performed at the receiver and a Precoding Matrix Indicator (PMI) is fed back to the transmitter as illustrated in Figure 2.9.

LAYER MAPPING

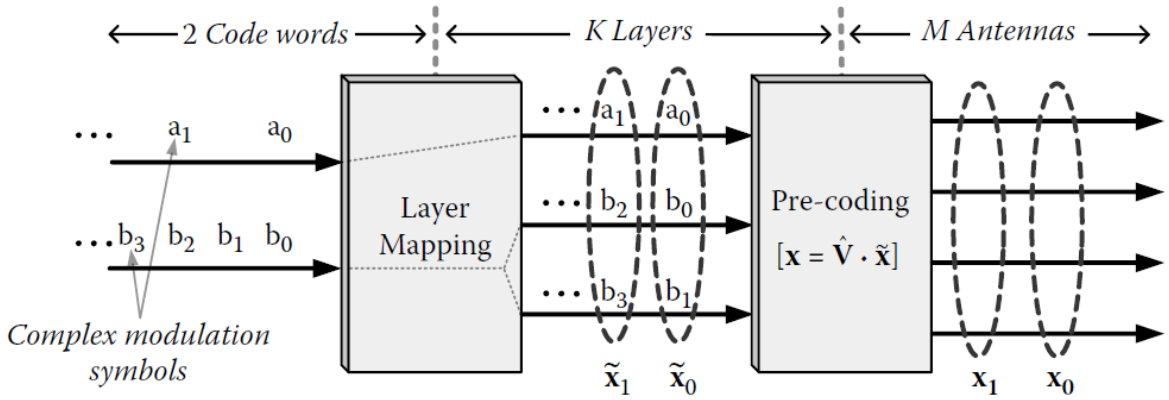

Fig. 2.10 Two codeword layer mapping

The objective of this procedure is to map different codewords onto the multiplexed spatial layers. In schemes with a single codeword, the modulation symbols are mapped to all the MIMO layers. In a situation where the number of codewords is equal to the rank of the channel matrix, a one-to-one mapping is implemented. When the number of codewords is less than the rank as is illustrated in Figure 2.10 , the layer mapping is more complicated. The layer mapping schemes implemented in LTE for a 4 antenna system are the 1-3 mapping and the 2-2 mapping [20]. In the 1-3 mapping codeword 1 is transmitted on layer 1 while codeword 2 is transmitted on 2, 3 and 4. In the 2-2 mapping codeword 1 is transmitted on layer 1 and 2 while codeword 2 is transmitted on 3 and 4.

2.7.3 MIMO CAPACITY

The normalized capacity of a $N_T \times N_R$ MIMO system is given by [21]:

$$C_{MIMO} = \mathbb{E}\left[log_2 \det(I_N + \frac{\rho}{N_T} HH^T)\right] bps/Hz \tag{2.17}$$

where ρ is the received SNR at each receiver antenna and $\mathbb{E}$ refers to the expectation. If σn are the singular values of the channel matrix $\mathbf{H}$,

$$C_{MIMO} = \mathbb{E}\left[\sum_{l=1}^{n_{min}} log_2\left(1+\frac{\rho}{N_T}\sigma_1^2\right)\right] \tag{2.18}$$

$$C_{MIMO} = \sum_{i=1}^{n_{min}} \mathbb{E}\left[log_2\left(1+\frac{\rho}{N_T}\sigma_1^2\right)\right] \tag{2.19}$$

where $n_{min} = min(N_T, N_R)$.

For a low SNR,

$$\log_2(1+x) \approx x log_2 e \tag{2.20}$$

thus,

$$C_{MIMO} = \sum_{i=1}^{n_{min}} \frac{\rho}{N_T}\mathbb{E}\left[\sigma_1^2\right]\log_2 e = M \times \rho \times log_2 e \tag{2.21}$$

For high SNR,

$$\log_2(1+x) \approx x log_2 x \tag{2.22}$$

Thus the capacity can be approximated by:

$$C_{MIMO} = \sum_{i=1}^{M} \mathbb{E}\left[\log_2\left(\frac{\rho}{M}\sigma_i^2\right)\right] \tag{2.23}$$

$$C_{MIMO} = n_{min} \times \log_2\left(\frac{\rho}{M}\right) + \sum_{i=1}^{M} \mathbb{E}\left[\log_2\left(\sigma_i^2\right)\right] \tag{2.24}$$

The capacity of a MIMO system scales linearly with the number of antennas at low SNR. At high SNR, the capacity scales with the degree of freedom n_{min}. However, the channel matrix needs to be full rank to provide this capacity scaling. If the full rank condition is compromised e.g. due to correlated antennas or line-of-sight propagation,

the capacity is limited. To solve the problem of rank reduction, the MIMO precoding process is implemented [19].

2.7.4 EFFECT OF CHANNEL STATE INFORMATION ON MIMO CAPACITY

This section illustrates the fact that channel knowledge can have a significant impact on the capacity of a MIMO system.

With perfect CSI at the receiver and none at the receiver, the MIMO capacity is [22]:

$$C_0 = B\ \mathbb{E}\left[\left| log\left(1+\frac{P}{N_t N_o B}HH^*\right)\right|\right] \tag{2.25}$$

where B is the bandwidth, N_o is the noise power and N_t is the number of transmission antennas.

$$C_0 = B\ \mathbb{E}\left[\sum_{i=1}^{min(N_t,N_r)} log\left(1+\frac{P}{N_t N_o B}\sigma_1^2\right)\right] \tag{2.26}$$

with perfect CSI at the transmitter, the capacity becomes,

$$C_0 = B\ \mathbb{E}\left[max\sum_{i=1}^{min(N_t,N_r)} log\left(1+\frac{P_i}{N_t N_o B}\sigma_1^2\right)\right] \tag{2.27}$$

The power allocation P_i is given by the water-filling algorithm [23]:

$$P_i = \left(\mu - \frac{N_o B}{\sigma_i^2}\right)^+ \tag{2.28}$$

where μ is the water-fill level. The optimal power allocation provides a maximum rate of:

$$C_* = B\ \mathbb{E}\left[\sum_{i=1}^{min(N_T,N_R)} \log\left(1+\frac{P}{\min(N_T,N_R)N_0 B}\sigma_i^2\right)\right] \tag{2.29}$$

The difference in capacity, $\Delta C = C_1 - C_0$, can be expressed as:

$$\Delta C = (C_1 - C_*) + (C_* - C_0) \tag{2.30}$$

where $(C_1 - C_*)$ is the water filling gain and $(C_* - C_0)$ is a directional gain.

2.8 CHANNEL MODEL

Channel modeling has a crucial role in the research and development of radio wireless systems. It helps in the design and simulation of mobile communication systems. Channel models can be categorized into two major classes; physical and analytical models.

Analytical models characterize the channel using its statistical properties without considering the wave propagation. Popular analytical models are correlation based models in which the channel matrix is described in terms of the spatial, frequency and temporal correlations. Research in advanced wireless techniques such as beamforming and spatial multiplexing require the integration of more detailed parameters. Such characterization can be provided by physical channel models, in which the channel is characterized by describing the multi-path propagation environment between the transmitter and the receiver [24]. Physical models incorporate radio wave propagation parameters such as such as Angle of Arrival (AOA), Angle of Departure (AOD) and Direction of Arrival (DOA). Depending on the degree of detail required, physical models can include polarization and time variation parameters.

For purposes of design, simulation and comparative analysis of MIMO systems and algorithms, standard channel models have been defined with the objective of establishing reproducible channel conditions. Examples of these reference models are the Spatial Channel Model (SCM), Spatial Channel Model Extended (SCME) and the Wireless World Initiative New Radio (WINNER) II models.

2.8.1 THE WIRELESS FADING CHANNEL

Wireless channel transmissions consist of a transmitter and a receiver physically separated by a radio propagation path. One possible path is formed through the direct

line-of-sight propagation while others are formed through reflection, diffraction and refractions from the ground, buildings, hills and other irregularities within the propagation environment. Each of these paths suffers from attenuation, distortion, noise and other impairments. The signal at the receiver is the vector sum of the different components arriving through multiple paths. These signal components cause interference which can be additive or multiplicative and this leads to a variation of the signal amplitude in time and frequency, a phenomenon known as fading. Large scale fading occurs as a result of signal attenuation caused by path loss or shadowing by large objects. Path loss represents the overall attenuation due to distance and is given by:

$$L_F = \left(\frac{4\pi rf}{c}\right)^2 \tag{2.31}$$

Shadowing is the signal loss that occurs when large objects obstruct the line-of-sight path between the transmitter and receiver. It occurs at a faster rate than path loss and has a Gaussian distribution.

Small scale fading refers to the rapid variation of the signal amplitude as the UE moves within the radio propagation environment. This type of fading occur as a result of the constructive and destructive interference of the signal components arriving at the receiver via multiple paths. A number of parameters play an important role in the characterization of fading, among these are the delay spread and the Doppler spread [25].

2.8.2 DELAY SPREAD

Let τ_k denote the channel delay for the k^{th} path while a_k is the amplitude and $P(\tau_k)$ is the power. The delay spread is expressed as:

$$\sigma_t = \sqrt{\hat{\tau}^2 - \tau^2} \tag{2.32}$$

where:

$$\hat{\tau} = \frac{\sum_k a_k^2 \tau_k^2}{\sum_k a_k^2} \tag{2.33}$$

and τ the excess delay is given by:

$$\tau = \frac{\sum_k a_k^2 \tau_k}{\sum_k a_k^2} \tag{2.34}$$

The coherence bandwidth B_c is inversely proportional to the delay spread.

$$B_c \propto \frac{1}{\sigma_t} \tag{2.35}$$

2.8.3 DOPPLER SPREAD

The complex amplitude a_k can be expressed as:

$$a_k(t) = \alpha_k \exp^{j(2\pi f_k t + \Phi_k)} \tag{2.36}$$

where α_k is the path loss, f_k is the Doppler frequency shift of the k^{th} path,Φ_k is the phase offset of the k^{th} multipath component respectively.The Doppler frequency shift is given by:

$$f_k = f_c \frac{v}{c_0} \cos(\theta_k) \tag{2.37}$$

where f_c is the carrier frequency, v is the mobile terminal velocity, c_0 is the speed of light and θ_k is the is the angle between the k^{th} incident ray and the MT moving direction. The largest difference between the Doppler shift frequencies, denoted as D_s, is known as the Doppler spread:

$$D_s = \max_{k,j} \left| f_k - f_j \right| \tag{2.38}$$

where f_k is the Doppler shift of the k^{th} path. The coherence time T_c is inversely proportional to the Doppler spread i.e.

$$T_c \propto \frac{1}{D_s} \tag{2.39}$$

2.8.4 TIME SELECTIVE FADING

As a result of frequency dispersion, the transmitted signal may undergo slow or fast fading. Contingent on the Doppler spread value, the LTE channel can be regarded as block fading or fast fading. In a block fading channel, the coherence time is larger than the subframe duration of $1ms$. In contrast, the fast fading channel has a coherence time that is smaller than the subframe duration. For a block fading scenario, the channel remains constant for the duration of a subframe while in a fast fading scenario, the channel is varying within a subframe.

2.8.5 FREQUENCY SELECTIVE FADING

As a result of time dispersion, the transmitted signal may undergo frequency flat or frequency selective fading. In a flat fading channel, the amplitude is constant for all signal frequency components while in a frequency selective channel, the amplitude varies with the frequency. The transmitted signal is subject to frequency selective fading if the LTE subframe duration is less than the delay spread of the channel τ_t.

2.8.6 STOCHASTIC MODEL OF FADING

In the stochastic model of the fading channel, the electromagnetic field of the received signal at a UE is represented by a scattering process. As the mobile user moves within the radio propagation environment, the incident plane-waves undergo a Doppler shift. Let $x(t)$ denote the transmitted signal, the corresponding transmitted passband signal is

given by:

$$\hat{x}(t) = Re\left[x(t)e^{j2\pi f_c t}\right] \tag{2.40}$$

The transmitted signal passes through a channel with L many different paths with each path having a corresponding Doppler shift. The received signal can be expressed as:

$$\hat{y}(t) = Re\left[\sum_{l=1}^{L} \alpha_l e^{j2\pi(f_c+f_l)(t-\tau_l)}\right] \tag{2.41}$$

where α_l, f_l, τ_l are the channel gain, Doppler shift and delay shift for the l^{th} path respectively. The received signal can be expressed as:

$$y(t) = \sum_{l=1}^{L} \alpha_l e^{j\Psi} x(t-\tau_l) \tag{2.42}$$

Where,

$$\Psi = \left\{2\pi(f_c + f_l\tau_l) - f_l\tau_l\right\} \tag{2.43}$$

The channel can be modeled as a linear time varying filter with a impulse response given by:

$$h(t,\tau) = \sum_{l=1}^{L} \alpha_l e^{j\Psi}\delta(t-\tau_l) \tag{2.44}$$

The path delays can be approximated as $\hat{\tau}$ hence:

$$h(t,\tau) = h(t)\delta(t-\hat{\tau}) \tag{2.45}$$

Where,

$$h(t) = \sum_{l=1}^{L} \alpha_l e^{j\Psi} \tag{2.46}$$

The received signal $\hat{y}(t)$ can thus be expressed as:

$$\hat{y}(t) = Re\left[y(t)e^{j2\pi f_c t}\right] \tag{2.47}$$

$$\hat{y}(t) = Re\left[\left(h_I(t) + jh_Q(t)\right)e^{j2\pi f_c t}\right] \tag{2.48}$$

$$\hat{y}(t) = h_I(t)\cos 2\pi f_c t + h_Q(t)\sin 2\pi f_c t \tag{2.49}$$

where $h_I(t)$ and $h_Q(t)$ are the in-phase and quadrature phase components of $h(t)$ respectively and are given by:

$$h_I = \sum_{l=1}^{L} \alpha_l \cos_l(t) \tag{2.50}$$

and

$$h_Q = \sum_{l=1}^{L} \alpha_l \sin_l(t) \tag{2.51}$$

If the number of paths, L, is large, the wireless channel has many scatterers and the amplitude of the received signal follows a Rayleigh distribution. The power spectrum density of the fading process is given by the Fourier Transform of the autocorrelation function of $\hat{y}(t)$ and is expressed as [15]:

$$R_{\hat{y}\hat{y}} = \frac{\Omega_p}{4\pi f_m \sqrt{1 - \left(\frac{f - f_c}{f_m}\right)^2}} \tag{2.52}$$

where

$$\Omega_p = \sum_{l=1}^{L} \alpha_l^2 \tag{2.53}$$

The power power spectrum density is referred to as the Doppler spectrum.

If the fading channel has dominant scattering components, the amplitude of the received signal follows the Rician distribution. The strongest component usually corresponds to the line-of-sight (LOS) component.

2.8.7 SISO CHANNEL MODEL

The short term fading Single Input Single Output (SISO) outdoor fading channel is characterized by time variation of the channel gain, subject to the MT terminal speed. The time variation of the channel is governed by the Doppler spread, which determines the time domain correlation of the channel.

JAKES MODEL

In the Jakes model, a Rayleigh fading channel subject to a given Doppler spread can be generated as a weighted sum of complex sinusoids [26]. It is assumed that the rays of the scattered components arriving from uniform directions are approximated by plane waves. The output of the Jakes model is a vector sum of an in-phase component and a quadrature component [27].

$$h(t) = \frac{E_0}{\sqrt{2N_0+1}}\Big(h_I(t) + h_Q(t)\Big) \tag{2.54}$$

where E_0 is a scaling constant,

$$h_I(t) = 2\sum_{n=1}^{N_0}\Big(\cos_n \cos \omega_N t\Big) + \sqrt{\cos_n \cos \omega_d t} \tag{2.55}$$

and,

$$h_Q(t) = 2\sum_{n=1}^{N_0}\left(\sin_n \sin \omega_n t\right) + \sqrt{\sin_N \sin \omega_d t} \tag{2.56}$$

ω_n and ω_N are the initial phases of the n^{th} Doppler shifted sinusoid and of the maximum Doppler frequency respectively. The in-phase and quadrature components have the following property:

$$\mathbb{E}\left\{\left(\frac{E_0 h_I(t)}{\sqrt{2N_0+1}}\right)^2\right\} = \mathbb{E}\left\{\left(\frac{E_0 h_Q(t)}{\sqrt{2N_0+1}}\right)^2\right\} = \frac{E_0^2}{2} \tag{2.57}$$

Thus the in-phase and quadrature components are statistically independent with an average power of $\frac{E_0^2}{2}$.

RAY BASED CHANNEL MODEL

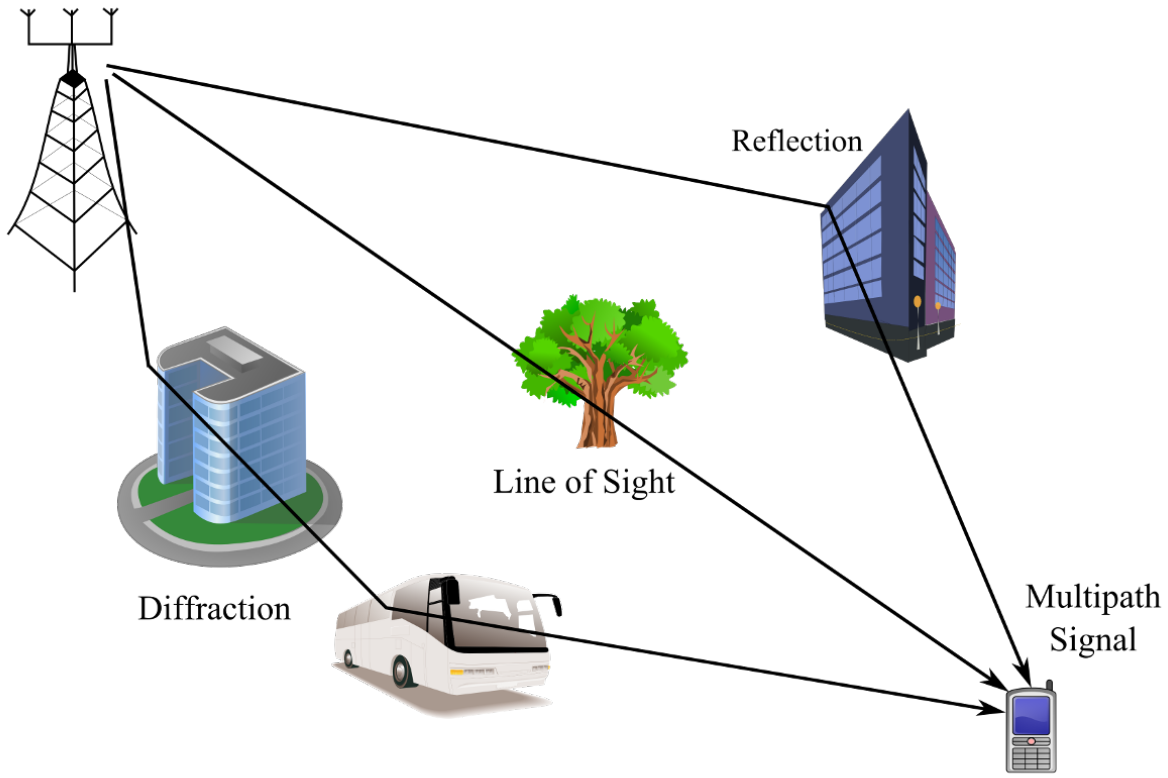

Fig. 2.11 Ray Tracing Model of Wireless Channel

The ray tracing method is a widely implemented technique in the design and modeling of wireless channels [25, 28]. Ray tracing techniques can be categorized into two main types; the imaging and the ray launching technique. The imaging technique, illustrated in Figure 2.11, borrows from the equivalent optical propagation method. It determines the propagation characteristics from a combination of parameters among which are the propagation distance, the incident angle of reflection and the permittivity of the reflection surface. The ray launching technique determines the propagation

characteristics using rays launched discretely at regular intervals then searching for rays arriving at the received position.

2.8.8 MIMO CHANNEL MODEL

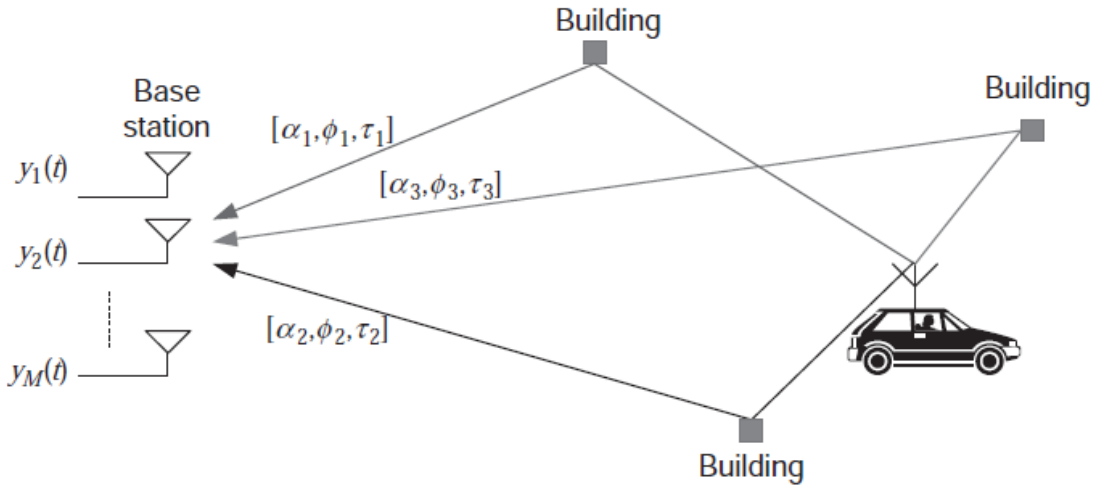

Fig. 2.12 MIMO Channel with Uniform Linear Array

Consider a MIMO channel in which the transmitter has a uniform linear array (ULA) of M antennas separated by an equal distance d as illustrated in Figure 2.12. The received signal vector can be expressed as [15]:

$$y(t) = \sum_{l=1}^{L} \alpha_l C(\Phi_i) x(t-\tau_l) + N(t) \tag{2.58}$$

where α_l, τ_l, Φ_l are the gain, delay and AOA for the l^{th} element respectively and $C(\Phi_l)$ is the steering vector defined as:

$$C(\Phi) = \left[C_1(\Phi), C_2(\Phi), C_3(\Phi), ..., C_M(\Phi)\right] \tag{2.59}$$

The received signal can be represented in integral form as:

$$y(t) = \int\int C(\Phi) h(\Phi,\tau) x(t-\tau) d\Phi + N(t) \tag{2.60}$$

where $h(\Phi, \tau)$ is the channel impulse response as a function of the Azimuth Delay Spread (ADS). The Power Azimuth Delay Spread (PADS) is given by:

$$P_i(\Phi, \tau) = \sum_{l=1}^{L} \alpha^2 \delta(\Phi - \Phi_l, \tau - \tau_l) \tag{2.61}$$

The Power Azimuth Spectrum (PAS) is expressed as:

$$P_A(\Phi) = \int P(\Phi, \tau) d\tau \tag{2.62}$$

The Azimuth Spread (AS) is defined by the central moment of the PAS and it is given by:

$$\sigma_A = \sqrt{\int (\Phi - \Phi_0)^2 P_A(\Phi) d\Phi} \tag{2.63}$$

where Φ_0 is the average AOA. The power delay spectrum is expressed as:

$$P_D(\tau) = \int P(\Phi, \tau) d\Phi \tag{2.64}$$

The delay spread is defined as the central moment of the Power Delay Spectrum (PDS) and it is expressed as:

$$\sigma_D = \sqrt{\int (\tau - \tau_0)^2 P_D(\tau) d\tau} \tag{2.65}$$

where τ_0 is the average delay spread.

MIMO channels are typically modeled using a statistical approach. The 3GPP has adopted the Kronecker model as the MIMO model for link level channel simulations [29]. The basic premise behind the Kronecker model is that the transmitter and receiver correlation matrices can be separated. The channel matrix for the Kronecker model is given by [30]:

$$\mathbf{H} = \mathbf{R}_t^{\frac{1}{2}} \mathbf{H}_{iid} \mathbf{R}_r^{\frac{1}{2}} \tag{2.66}$$

where $\mathbf{R}_t = \mathbb{E}\left[\mathbf{H}\mathbf{H}^H\right]$ and $\mathbf{R}_r = \mathbb{E}\left[\mathbf{H}\mathbf{H}^H\right]$ are the transmitter and receiver correlation matrices respectively and $\mathbf{H}_{\mathbf{iid}}$ represents an independent and identically distributed Rayleigh fading channel with zero mean Gaussian entries.

THE WINNER II CHANNEL MODEL

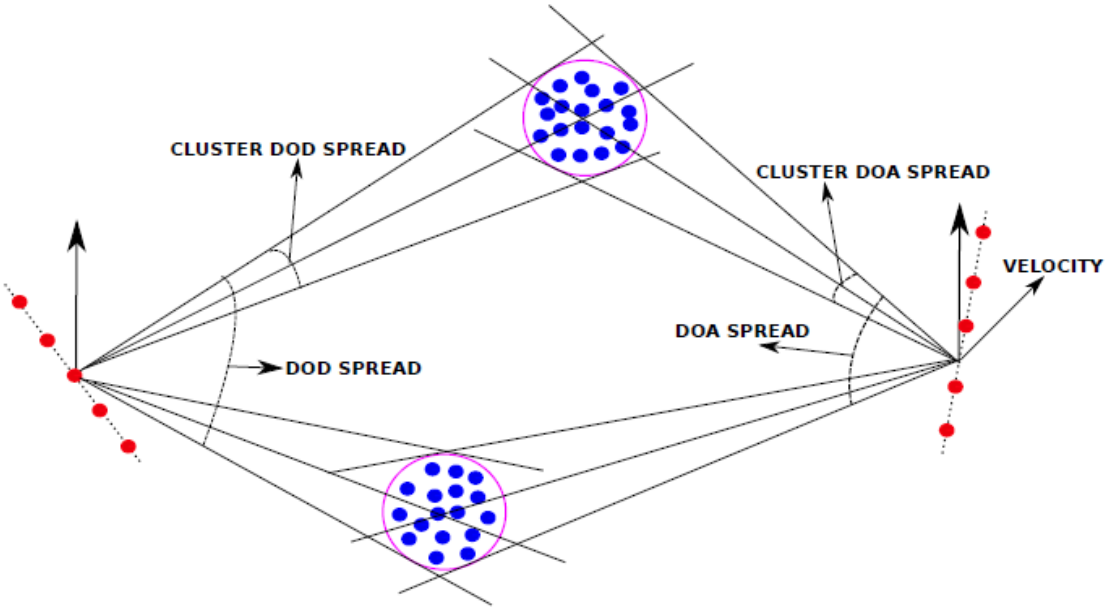

Fig. 2.13 WINNER Channel with cluster of scatterers

The WINNER model, as illustrated in Figure 2.13, is a ray based model in which the channel is modeled as a summation of multipath components referred to as clusters [31, 32]. The MIMO channel matrix is expressed as:

$$\mathbf{H}(t,\tau) = \sum_{p=1}^{P} \mathbf{H}_p(t,\tau)\delta(\tau - \tau_p) \tag{2.67}$$

where P is the number of clusters.

The spatial, temporal and frequency correlations are an important aspect of a MIMO channel. These properties will be presented here for the WINNER II channel model [33].

SPATIAL-TEMPORAL CORRELATIONS

Let $\mathbf{h}_{nm}$ denote the impulse response of the channel between the transmitter antenna m and the receiver antenna n. The spatial-temporal correlation between two channel coefficients for a time interval Δt is expressed as:

$$\rho_{st} = \mathbb{E}\left\{ \frac{\mathbf{h}_{n_1 m_1}(t)\mathbf{h}^H_{n_2 m_2}(t+\Delta t)}{\sqrt{\left|\mathbf{h}_{n_1 m_1}(t)\right|^2 \left|\mathbf{h}_{n_2 m_2}(t)\right|^2}} \right\} \tag{2.68}$$

SPATIAL CORRELATIONS

The spatial correlation function can be determined from the spatial-temporal correlation function as:

$$\rho_s(d_r, d_t) = \rho_{st}\Big|\Delta t = 0 \tag{2.69}$$

The spatial correlation depends on the AOA and on the AOD.

TEMPORAL CORRELATIONS

The temporal correlation function can be obtained as:

$$\rho_t(\Delta t) = \rho_{st}\Big| d_r = d_t = 0 \tag{2.70}$$

$$\rho_t(\Delta t) = \sum_{p=1}^{P} \mathbb{E}\left\{ e^{jk(v_{p,q}\Delta t)} \right\} \tag{2.71}$$

The temporal correlation function is dependent on the Doppler shifts and the time interval.

FREQUENCY CORRELATIONS

The frequency correlation function can be determined from the average power delay profile as:

$$\rho_f = \frac{\sum_{p=1}^{P} a_p e^{-j2\pi\tau_p\Delta_f}}{\sum_{p=1}^{P} a_p} \tag{2.72}$$

where Δf is the frequency spacing.

2.9 LINK ADAPTATION

In order for LTE to meet its specified spectral efficiencies, it utilizes channel aware link adaptation in which the system parameters are dynamically varied to adapt to changing channel conditions. Among the parameters that are dynamically adapted are the PMI used to select the precoding matrix, the Rank Indicator (RI) which determines the number of transmission layers or rank and the Channel Quality Indicator (CQI) modulation and coding scheme(MCS) [34]. Dynamic tuning of the system parameters enables effective use of the available bandwidth.

2.9.1 CHANNEL QUALITY INDICATOR

Table 2.3 Channel quality indicator in terms of the modulation scheme and coding rate

CQI	Modulation Scheme	Coding Rate unit of(1/1024)	Bit per Symbol
0	QPSK	0	0.00
1	QPSK	78	0.15
2	QPSK	120	0.23
3	QPSK	193	0.38
4	QPSK	308	0.60
5	QPSK	449	0.88
6	QPSK	602	1.18
7	16-QAM	378	1.48
8	16-QAM	490	1.91
9	16-QAM	616	2.41
10	64-QAM	466	2.73
11	64-QAM	567	3.32
12	64-QAM	666	3.90
13	64-QAM	772	4.52
14	64-QAM	873	5.12
15	64-QAM	948	5.5513

The Channel Quality Indicator (CQI) is a 4 bit parameter that provides a measure of the channel quality. It indicates the highest data rate that the UE can handle for a target Block Error Rate (BLER) of 10% [34]. The CQI depends mainly on the received signal to interference noise ratio (SINR). The BS uses the CQI feedback parameter to determine the modulation and coding scheme (MCS) according to the mapping shown

in Table 2.3. The CQI parameter is also utilized in in channel aware scheduling to share radio resources among multiple UEs.

2.9.2 PRECODING MATRIX INDICATOR

MIMO systems can enhance their capacity through channel knowledge at the transmitter. In LTE the channel state is determined through feedback from the UE to the BS. The feedback for the complete MIMO channel can create excessive overhead reducing the effective bandwidth. For instance, in a 4x4 MIMO system, there would be a need to feedback the channel state for the 16 different paths between the transmitter and receiver. To reduce the feedback overhead, a finite set of precoding matrices called a codebook is selected for each MIMO configuration. The codebook is known to both the UE and the BS and once the UE performs channel estimation, it selects the most appropriate matrix from the codebook then feeds back the PMI to the BS. There are a variety of techniques for PMI selection with emphasis on different performance metrics [35].

2.9.3 RANK INDICATOR

The RI parameter denoted the number of layers used for a spatial multiplexing system. In LTE this parameter is used to estimate the rank of the channel matrix and thus the number of feasible layers. The are a number of different criteria available in the literature for determining the rank depending on different metrics and criteria [36].

2.10 CALCULATION OF FEEDBACK PARAMETERS

Three feedback parameters, CQI, PMI and RI are computed from the channel estimate or channel prediction value and then sent back to the transmitter. There are various methods in the literature for calculating these parameters. In this section, the methods used in this research work are presented.

2.10.1 CHANNEL QUALITY INDICATOR

The CQI value is chosen to achieve a given BLER target which is 10% for LTE. The Effective SINR Mapping (ESM) [37] maps the instantaneous channel state into the effective Signal to Interference Noise Ratio (SINR) which is then used to calculate a BLER corresponding to the channel state. There are two ESM techniques: the Mutual Information Effective SINR Mapping (MIESM) and the Exponential Effective SINR Mapping (EESM). The mapping in the EESM technique given by [38]:

$$SINR_{eff} = \beta f^{-1}\left(\frac{1}{R}\sum_{r=1}^{R} f\left(\frac{SINR_r}{\beta}\right)\right) \tag{2.73}$$

The β values are then calibrated to determine the CQI corresponding to the channel state [39]. The SINR to CQI mapping used in this research work is illustrated in Table 2.4.

Table 2.4 SINR to CQI Mapping

SINR in dB	-50.00	-6.91	-5.15	-3.18	-1.25	0.76	2.70	4.69
CQI	0	1	2	3	4	5	6	7
SINR in dB	6.53	8.57	10.37	12.3	14.18	15.9	17.8	19.83
CQI	8	9	10	11	12	13	14	15

2.10.2 PRECODING MATRIX INDEX

When MIMO precoding is used, the input output relationship of the MIMO system an time n for subcarrier k becomes:

$$\mathbf{y}_{n,k} = \mathbf{H}_{n,k}\mathbf{W}_i\mathbf{x}_{n,k} + \mathbf{z}_{n,k} \tag{2.74}$$

where $\mathbf{W}_i \in \mathcal{W}$ is the precoding matrix, $\mathcal{W}$ is the set of matrices defined in the codebook and i is the index of the matrix within this codebook. The precoding matrix will be a

single value for the entire subframe and all subcarriers. The capacity of each subcarrier in bits per channel is given by [40]:

$$I_k(W_i) = \log_2 \det\left(I_L + \frac{1}{\sigma^2} W_i^H H_k^H W_i H_k \right) \tag{2.75}$$

To determine the optimal precoder for the entire bandwidth of K subcarriers, the mutual information on every subcarrier is summed and then maximized with respect to the precoding matrix as [41]:

$$W_j = \sum_{k=1}^{K} \sum_{n=1}^{N} I_{n,k}(W_i) \tag{2.76}$$

where $I_{n,k}$ is the mutual information of the resource element. The index j of the optimal precoder W_j is then the PMI that is fed back to the transmitter.

2.10.3 RANK INDICATOR

The RI is chosen based on the maximum channel capacity criterion. The mutual information can be expressed in terms of the SINR as [42]:

$$I_{n,k} = \sum_{l=1}^{L} \log_2 \left(1 + SINR_{n,k,l} \right) \tag{2.77}$$

where L is the number of spatial transmission layers. The optimal RI is the number of layers that maximizes the mutual information. A layer number L can only be combined with a precoding matrix from the corresponding codebook $\mathcal{W}_L$.

2.11 CHANNEL AGING

Channel aging refers to the mismatch between the channel state at the instant the UE performs channel measurement and the instant the feedback parameters are used by the BS for link adaptation and scheduling.

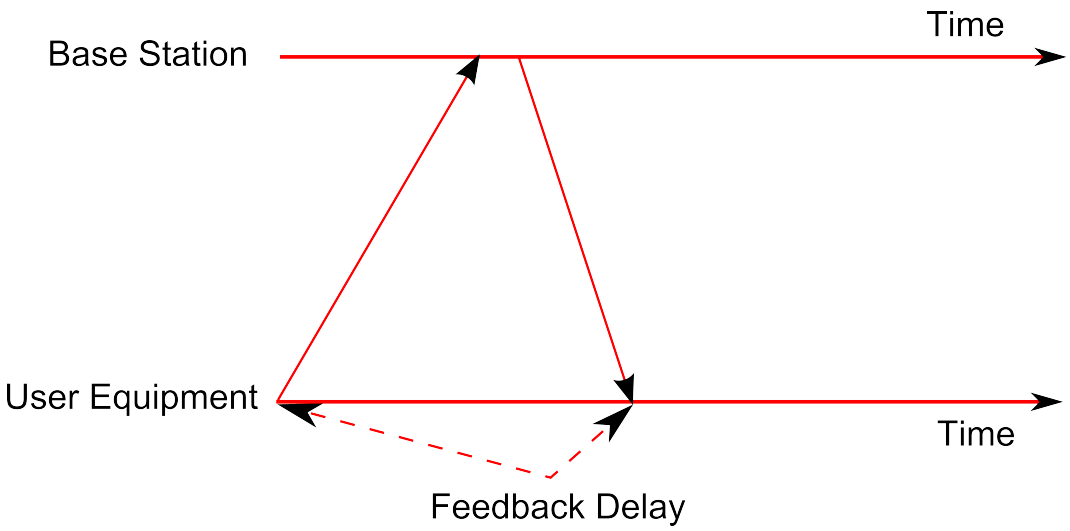

Fig. 2.14 Channel Aging

As illustrated in Fig 2.14 there is a time delay between the instant the MT sends the CSI feedback and the time the MT receives the data from the BS. Channel aging results in inaccurate link adaptation and scheduling eventually causing a reduction in overall system throughput [43, 44].

2.12 CHANNEL ESTIMATION

Multiple input multiple output techniques which employ multiple transmitter and receiver antennas can be used to enhance the performance of an OFDM system either by improving the reliability of the radio link in the presence of fading or more importantly by increasing the data rate through spatial multiplexing. MIMO techniques offer spatial multiplexing capabilities in which the system capacity has the ability to scale linearly with the number of antennas used in the MIMO configuration. This linear scaling however depends on whether the channel state can be obtained at the receiver[45]. The channel state at the receiver can be estimated through pilot symbols, blind or semi blind channel estimation. In pilot based channel estimation, symbols known to both the transmitter and receiver and transmitted along with the data symbols. Depending on how these pilots are inserted into the bit stream, block type or comb type pilot structures

can be implemented. Blind channel estimation uses the statistical properties of the received signals without requiring the use of pilots [46]. Semi-blind estimation [47] combines the use of pilots alongside the statistical properties. For comb-type pilot based estimation, the channel matrix is estimated at the pilot intervals and interpolation is used at non-pilot intervals [48]. The structure of the pilots within a RB for an LTE MIMO is contingent on the number of antennas used at the transmitter. For a MIMO configuration using four transmitter antennas, each RB at the first and second antennas contain four pilot symbols while in the third and fourth antennas there are two pilots per RB. For purposes of channel estimation, the MIMO channels can be assumed to have low correlation and thus can be considered independent single input single output (SISO) channels. The comb-type pilot configuration provides better performance compared to the block-type in fast fading channels [49].

2.12.1 PERFECT ESTIMATOR

The channel can be estimated perfectly if all the transmitted symbols are known at the receiver. This is not possible for practical systems but in a simulated environment such an estimator can be created. This perfect estimator is used as a benchmark for the other algorithms presented in this paper.

2.12.2 LS CHANNEL ESTIMATOR

The least-square (Least Squares (LS)) estimator method calculates the filter coefficient in order to minimize a cost function given by [15]:

$$\begin{aligned} J(\hat{\mathbf{H}}) &= \|\mathbf{Y}-\mathbf{X}\mathbf{H}\|^2 \\ &= (\mathbf{Y}-\mathbf{X}\hat{\mathbf{H}})^H(\mathbf{Y}-\mathbf{X}\hat{\mathbf{H}}) \end{aligned} \tag{2.78}$$

where H is the channel matrix, Y is the received vector and X is a diagonal matrix comprised of the transmitted symbols. Setting the derivative with respect to $\hat{H}$ to zero,

$$\frac{\partial J(\hat{\mathbf{H}})}{\partial \hat{\mathbf{H}}} = -2(\mathbf{X^H H})^* + 2(\mathbf{X^H X}\hat{\mathbf{H}})^* = 0 \tag{2.79}$$

which reduces to,

$$\mathbf{X^H X}\hat{\mathbf{H}} = \mathbf{X^H Y} \tag{2.80}$$

The LS channel prediction solution can therefore be expressed as:

$$\hat{\mathbf{H}}_{ls} = (\mathbf{X}^H\mathbf{X})^{-1}\mathbf{X}^H\mathbf{Y} = \mathbf{X^{-1}Y} \tag{2.81}$$

2.12.3 MMSE CHANNEL ESTIMATION

$$\mathbb{E}\{\|\mathbf{e}\|^2\} = \mathbb{E}\{\left\|\hat{\mathbf{H}}_{mmse} - \mathbf{H}\right\|^2\} \tag{2.82}$$

Consider the LS solution of (2.81) and let $\mathbf{H}_{mmse} = \mathbf{W}\mathbf{H}_{ls}$, then from the orthogonality principle:

$$\begin{aligned}
\mathbb{E}\{e\mathbf{H}_{ls}^H\} &= \mathbb{E}\{(\mathbf{H} - \hat{\mathbf{H}}_{\mathbf{mmse}})\mathbf{H_{ls}}^H\} \\
&= \mathbb{E}\{(\mathbf{H} - \mathbf{W}\hat{\mathbf{H}}_{\mathbf{ls}})\mathbf{H_{ls}}^H\} \\
&= \mathbb{E}\{\mathbf{H}\hat{\mathbf{H}}_{\mathbf{ls}}\} - \mathbf{W}\mathbb{E}\{\hat{\mathbf{H}}_{\mathbf{LS}}\hat{\mathbf{H}}_{\mathbf{ls}}\} \qquad = 0
\end{aligned} \tag{2.83}$$

The weight matrix, $\mathbf{W}$, can therefore be expressed as:

$$\mathbf{W} = \mathbf{R}_{H\hat{H}_{ls}}\mathbf{R}^{-1}_{\hat{\mathbf{H}}_{ls}\hat{\mathbf{H}}_{ls}} \tag{2.84}$$

The autocorrelation matrix of $\hat{\mathbf{H}}_{ls}$ is given by:

$$\begin{aligned}
\mathbf{R}_{\hat{H}_{ls}\hat{H}_{ls}} &= \mathbb{E}\{\hat{\mathbf{H}}_{ls}\hat{\mathbf{H}}_{ls}^{H}\} \\
&= \mathbb{E}\{\mathbf{X}^{-1}\mathbf{Y}(\mathbf{X}^{-1}\mathbf{Y})^{H}\} \\
&= \mathbb{E}\{\mathbf{X}^{-1}(\mathbf{HX}+\mathbf{Z})(\mathbf{X}^{-1}(\mathbf{HX}+\mathbf{Z}))^{H}\} \\
&= \mathbb{E}\{\mathbf{HH}^{H}\}+\mathbb{E}\{\mathbf{X}^{-1}\mathbf{ZZ}^{H}(\mathbf{X}^{-1})^{H}\} \\
&= \mathbf{R}_{HH}+\sigma^{2}\mathbf{I}
\end{aligned} \tag{2.85}$$

$$\mathbf{H}_{mmse} = \mathbf{R}_{HH_{ls}}(\mathbf{R}_{HH}+\sigma^{2}\mathbf{I})^{-1}\mathbf{H}_{ls} \tag{2.86}$$

The LS and the MMSE algorithm have been widely applied for channel estimation in OFDMA systems [50, 51]. Research has shown better performance for the MMSE algorithm compared to the LS method which suffers from a high mean square error especially for low SINR values [48, 52]. The MMSE algorithm however has the disadvantage of having high computation complexity mainly due to matrix inversion. A number of techniques have been proposed to reduce the MMSE complexity. In [53], an iterative process is used to perform matrix inversion to reduce the complexity. In [5], the correlation matrix is reduced in size through down-sampling which then reduces the number of operations required to perform the inversion. A proposal to partition the autocorrelation matrix is made in [54] where the MMSE weight matrix is computed from the correlation of a subset of the nearest subcarriers rather than the entire set of subcarriers. This has the effect of reducing the matrix size and thereby the complexity of the inversion process.

2.12.4 DECISION DIRECTED CHANNEL ESTIMATION

The decision directed channel estimation technique as illustrated in Fig 2.15 uses the initially detected data symbols to perform channel estimation alongside the pilot symbols.

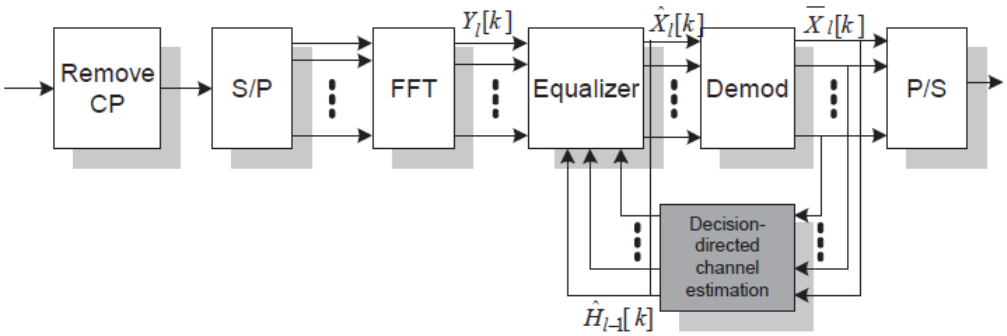

Fig. 2.15 Decision Directed Channel Estimation

The CSR signals or pilots used in conventional channel estimation are inserted within the time-frequency grid of the LTE system. These pilots are not adequate in high mobility scenarios due to the fact that the intervals between them is not short enough. In addition, channel estimation done exclusively through CSR signals does not utilize the channel information available at the receiver equalizer. Decision directed channel estimation can be used to enhance the performance by using the information extracted from data symbols as well as reducing the pilot overhead [55]. Once the initial estimation has been done using the pilot symbols, any subsequent channel estimation is done by using the detected symbol. Let $\hat{H}_n$ be the channel estimate made by using the n^{th} OFDM symbol, the n^{th} received symbol can be detected and equalized using the $(n-1)^{th}$ symbol, i.e.

$$\hat{X}_n = \frac{Y_n}{\hat{H}_{n-1}} \tag{2.87}$$

Let $\bar{H}_n$ denote the detected value for the equalized symbol $\hat{X}_n$, then the channel estimate for the n^{th} symbol is given by:

$$\hat{H}_n = \frac{Y_n}{\bar{X}_n} \tag{2.88}$$

2.13 CHANNEL PREDICTION

Channel prediction for OFDM systems has been shown to provide improved performance in terms of the overall capacity [43, 56–58]. Let h_n be the channel impulse response at time h_n, the channel predictor is required to predict the channel at time $n+D$, where D is the number of steps ahead required. The predicted channel can be formulated as a weighted sum of M previous values as follows:

$$h_{n+D} = \sum_{k=0}^{M-1} a_k h_{n-k-D} \tag{2.89}$$

The a_k parameters are dynamic for a fading channel and they must be dynamically adapted to the changing channel if the prediction is to be adequate.

2.14 CHANNEL PREDICTION METHODS

The basic premise of channel prediction methodologies is utilizing the knowledge of the current and past CSI to forecast a future channel state. In order to predict the future CSI values using past channel estimates, a prediction model is required. Existing channel prediction models can be classified into two broad categories: (I) Parametric Estimation Model and (II) Autoregressive Model.

2.14.1 PARAMETRIC RADIO CHANNEL MODEL

The prediction problem can be written in polynomial form as an FIR expressed as

$$z^L \hat{h}_n = \left(\sum_{i=0}^{n-1} a_i z^{-n} \right) h_n \tag{2.90}$$

when the polynomial $1 - z^{-L}\sum_{i=0}^{n-1} a_i z^{-i}$ has all zeros on the unit circle, the channel can be modeled as a sum of sinusoids [59] each having different amplitudes, Doppler frequencies and phase. Some common parametric techniques used in channel prediction are the subspace methods of Estimation of Signal Parameters via Rotational Invariance Techniques (ESPRIT) and MUltiple Signal Classification (MUSIC) [60].

2.14.2 AUTOREGRESSIVE MODEL

This model is based on the concept of computing the future channel as a weighted sum of the current and past channel estimates. The AR model requires a knowledge of the channel autocorrelation function and since this is not available it must be estimated from the noisy channel estimates. A common technique of doing this is by a solution of the Yule Walker equations [61, 62]. In the AR model the channel prediction D steps ahead is given by:

$$\hat{h}_{t+D} = a_0 h_t + a_1 h_{t-1} + ... + a_{m-1} h_{t-M+1} \tag{2.91}$$

The a_k parameters in (2.91) are time varying and are determined by prediction algorithms such as LS, MMSE and Recursive Least Squares (RLS).

2.15 PREDICTION ALGORITHMS

This section provides an overview of the MMSE algorithm which is the basis of the proposed method as well as two other prediction methods used in this thesis for comparative purposes.

2.15.1 NLMS CHANNEL PREDICTION

The normalized least mean square algorithm for channel prediction is:

$$\mathbf{W}[n+1] = \mathbf{W}[n] + \frac{\mu}{\left|\left|\mathbf{H}_{n-p}\right|\right|^2} \tag{2.92}$$

where μ is the adaptation constant, $e_{n,l}$ is the prediction error and,

$$\left|\left|\mathbf{H}_{n-p}\right|\right|^2 = \sum_{i=0}^{M-1} \left|\mathbf{H}_{n-p-i}\right|^2 \tag{2.93}$$

The NMLS algorithm requires $0 < \mu < 2$ for stable operation.

2.15.2 RLS CHANNEL PREDICTION

The update equation for the RLS algorithm is given by [63]:

$$\mathbf{W}[n] = \mathbf{W}[n-1] + k_n \varepsilon_n^* \tag{2.94}$$

where,

$$\varepsilon_n = \mathbf{H}_n - \mathbf{W}^H[n-1]\mathbf{H}_{n-p} \tag{2.95}$$

and $\mathbf{k}_n$ is the RLS gain vector given by:

$$\mathbf{k}_n = \frac{P_{n-1}\mathbf{H}_n}{\lambda + \mathbf{H}_n^H \mathbf{P}_{n-1}\mathbf{H}_n} \tag{2.96}$$

where,

$$\mathbf{P}_n = \frac{1}{\lambda}\mathbf{P}_{n-1}(\mathbf{I} - \mathbf{k}_n \mathbf{H}_n^H) \tag{2.97}$$

The initial value of $\mathbf{P}_n$ is set as:

$$\mathbf{P}_0 = \delta^{-1}\mathbf{I} \tag{2.98}$$

where δ is a stabilization factor and $0 < \delta < 1$.

2.15.3 MMSE PREDICTION

The prediction filter coefficients can be computed by use of the MMSE algorithm which minimizes the Mean Square Error (MSE). The prediction process MSE is given by:

$$MSE = \mathbb{E}\left[\left|H - \tilde{H}\right|^2\right] \tag{2.99}$$

minimizing the MSE results in the Wiener-Hopf equations[63]:

$$\mathbf{Ra} = \mathbf{r} \tag{2.100}$$

where **R** is the autocorrelation matrix and **r** is the matrix of cross-correlations.

$$\mathbf{a} = \left[a_1 a_2 \cdots a_M\right]^T \tag{2.101}$$

$$\mathbf{r} = \left[R_{xx}(1) R_{xx}(2) \cdots R_{xx}(M)\right]^T \tag{2.102}$$

$$\mathbf{R} = \begin{bmatrix} R_{HH}(0) & R_{HH}(1) & . & . & R_{HH}(1-M) \\ R_{HH}(1) & R_{HH}(2) & . & . & R_{HH}(2-M) \\ . & . & . & . & . \\ . & . & . & . & . \\ . & . & . & . & . \\ R_{HH}(M-2) & . & . & . & R_{HH}(1) \\ R_{HH}(M-1) & R_{HH}(M-2) & . & . & R_{HH}(0) \end{bmatrix} \tag{2.103}$$

where,

$\mathbf{R}_{HH}$ is the autocorrelation function $\mathbb{E}\{\mathbf{H}(n)\mathbf{H}(n-k)\}$.

2.16 RELATED WORK

The use of the MMSE criterion in channel estimation and prediction is extensive in the literature. In [64, 65], time domain MMSE channel prediction algorithms for a SISO system are presented while a frequency domain technique is presented in [66]. In [4, 67–69], the channel prediction algorithms treat the MIMO channel as consisting of independent SISO channels and thus only the temporal correlations are considered. In [70, 71], spatial and temporal correlations are incorporated in the prediction methodologies presented.

A major drawback of the MMSE algorithm is its high complexity mainly due to the real-time inversion a large matrix. Various methodologies have been proposed to reduce this complexity. In [72], the complexity reduction is achieved by first modeling the multipath channel as a linear combination of orthonormal basis vectors, then determining the Karhunen-Loeve (KL) expansion series coefficients. In [54, 64, 73], the authors tackle the problem by proposing methods to reduce the size of the filter weight matrix. An iterative method for matrix inversion is presented in [53] resulting in a more robust MMSE equalizer. In [74, 75], the MMSE matrix is separated into several matrices to corresponding to individual time and frequency or spatial filtering.

Channel prediction for fast fading SISO systems have been extensively studied previously in the literature [64, 66, 76]. Many of these utilize the AR model in which the predicted channel is obtained as a weighted sum of past estimates. The AR coefficients are determined using the MMSE algorithm. A number of studies have been reported on the channel estimation and prediction in MIMO-OFDM systems. In [4, 67, 69] the prediction utilizes the temporal correlations without any input from the spatial correlations among the different antennas to enhance the prediction. In [70, 71], the authors present a 2D-MMSE channel prediction technique which incorporates spatial and temporal correlations but is insensitive to frequency variations making it inadequate

for frequency selective channels. In [77, 78], 3D channel estimation techniques are presented which operate by incorporating the temporal, frequency and spatial correlations. The authors in [70, 71] have proposed MMSE based prediction techniques which exploit the temporal and spatial correlations but the presented methods still have the high complexity associated with the matrix inversion of the MMSE algorithm.

CHAPTER THREE

METHODOLOGY FOR CHANNEL PREDICTION

3.1 INTRODUCTION

Channel prediction is used to predict the future channel state from the current and past channel observations. The channel prediction technique can ether be parametric or non-parametric. Parametric predictors such as [79, 80] use deterministic channel models in their operation while non-parametric predictors use statistical channel models such as the AR model used in [81].

The simplified block diagram of the system employed in this thesis is shown in Figure 3.1. The model depicts a decision directed channel predictor in which the received symbols are used to perform channel estimation. The prediction value is then determined as a weighted sum of the current and past channel vectors.

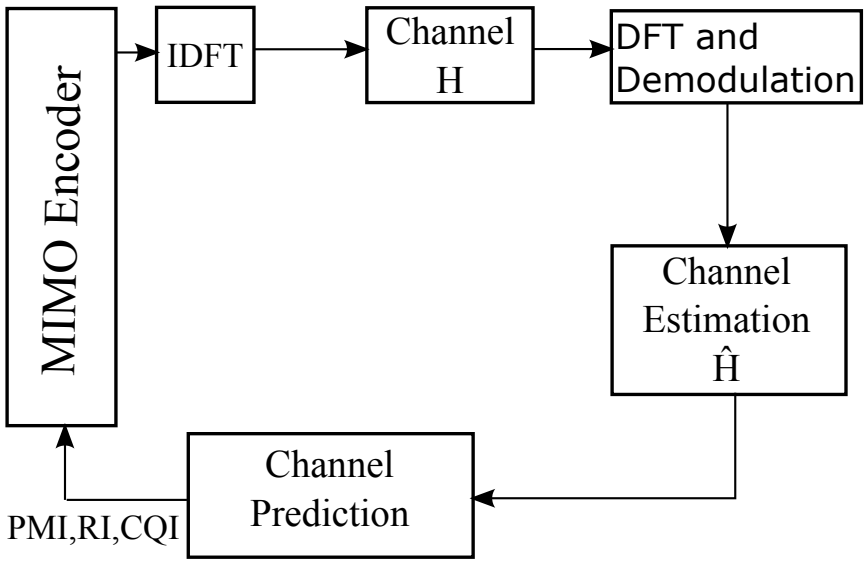

Fig. 3.1 Block diagram of Proposed Model for Channel Prediction in Block Fading Channels

A D step ahead channel prediction filter which computes the predicted channel matrix given the current and past received vectors $y_{n-D}, y_{n-D-1}, y_{n-D-M+1}$, where M is the filter memory is then developed. The predicted channel response is given by:

$$\tilde{\mathbf{H}}_{n+D} = \sum_{m=0}^{M-1} \mathbf{W}_{n,m} \hat{\mathbf{H}}_{n-m} \tag{3.1}$$

A decision directed process is proposed in which the received vector y_n is used to compute an estimate of the current channel matrix $\hat{\mathbf{H}}$. The current and past values of $\hat{\mathbf{H}}$ are then used in a prediction filter to determine the channel prediction value $\tilde{\mathbf{H}}$.

3.2 CHANNEL PREDICTION FOR BLOCK FADING

The channel prediction algorithm developed for block fading channels is discussed in this section. In a block fading radio channel, the coherence time of the channel has a duration whose length is larger than one LTE subframe of 1 ms. This means that the CIR remains constant for the entire subframe. The coherence time is given by [82]:

$$T_s = \frac{1}{4D_s} \tag{3.2}$$

where D_s is the Doppler spread. For a carrier frequency of 2.3 GHz, assuming Jakes Model with $D_s = 2f_{s_{max}}$, the maximum Doppler shift for block fading is $f_{s_{max}}$ = 125 Hz at a user velocity of 17 m/s. In order to exploit the temporal correlations, the filter memory, M, must be greater than the channel coherence time [54].

3.2.1 SYSTEM MODEL

An OFDM-MIMO system with K subcarriers, N_T transmit antennas and N_R receive antennas is considered. An input bit stream d_n is modulated, encoded and mapped to

a symbol. The frequency domain sequence from the i^{th} transmit antenna during the n^{th} OFDM symbol is denoted as $\mathbf{x}_{n,i,k}$ where k is the subcarrier index. The sequence received by the j^{th} receive antenna is given by:

$$\mathbf{y}_{n,j,k} = \sum_{n=1}^{N_T} \mathbf{h}_{n,j,i,k}\mathbf{x}_{n,i,k} + \mathbf{z}_{n,j,k} \tag{3.3}$$

where $\mathbf{h}_{n,j,i,k}$ is the frequency response of the channel between the i^{th} transmit antenna and the j^{th} receive antenna for the k^{th} subcarrier during the n^{th} LTE subframe and $\mathbf{z}_{n,j,k}$ is the AWGN with a variance of β^2. The signal transmitted on the k^{th} subcarrier from all the N_T transmit antennas during the n^{th} subframe is given by:

$$\mathbf{X}_{n,k} = \begin{bmatrix} \mathbf{x}_{n,1,k} & . & . & . & \mathbf{x}_{n,N_T,k} \end{bmatrix}^T \tag{3.4}$$

The received signal can be expressed as:

$$\mathbf{Y}_{n,k} = \mathbf{H}_{\mathbf{n},\mathbf{k}}\mathbf{X}_{\mathbf{n},\mathbf{k}} + \mathbf{Z}_{\mathbf{n},\mathbf{k}} \tag{3.5}$$

where,

$$\mathbf{Z}_{n,k} = \begin{bmatrix} \mathbf{z}_{n,1,k} & . & . & . & \mathbf{z}_{n,N_T,k} \end{bmatrix}^T, \tag{3.6}$$

$$\mathbf{Y}_{n,k} = \begin{bmatrix} \mathbf{y}_{n,1,k} & . & . & . & \mathbf{y}_{n,N_T,k} \end{bmatrix}^T, \tag{3.7}$$

$$\mathbf{H}_{n,k} = \begin{bmatrix} h_{n,1,1,k} & . & . & . & h_{n,1,N_T,k} \\ . & . & & & . \\ . & & . & & . \\ . & & & . & . \\ h_{n,N_R,1,k} & . & . & . & h_{n,N_R,N_T,k} \end{bmatrix} \tag{3.8}$$

For all K subcarriers, the general system description is given by:

$$\mathbf{Y}_n = \mathbf{H}_n\mathbf{X}_n + \mathbf{Z}_n \tag{3.9}$$

The system model is valid for block fading channels where the channel remains constant for one subframe duration.

3.2.2 APPROXIMATE MMSE CHANNEL PREDICTION ALGORITHM

The complexity of the MMSE channel prediction algorithm is brought about by the inversion of a $KN_TN_RM \times KN_TN_RM$ matrix. The proposed algorithm reduces the complexity by:

(a) reducing the matrix size through down-sampling

(b) approximating the matrix inversion through iteration

3.2.3 MATRIX SIZE REDUCTION

The matrix size reduction is performed in a series of steps according to the method set out in [83] as follows:

(i) Choose a down-sampling factor value L where $L \ll K$ and $K \mid L$.

(ii) Sample the channel matrix every L^{th} sample and create a reduced matrix of size $M = \frac{K}{L}$ from the sampled elements given by:

$$\mathbf{H}_s = \left[\mathbf{H}_{s,1}^T, ..., \mathbf{H}_{s,M}^T\right]^T \tag{3.10}$$

(iii) Calculation of the MMSE matrix by using the a subset of the sampled subcarriers instead of using the correlation between all subcarriers. This results in the

calculation of an autocorrelation matrix $\mathbf{R}_{HH}^{s}$ of dimension $M \times M$ as:

$$\mathbf{R}_{HH}^{(s)} = \mathbb{E}\left\{\mathbf{H}_s \mathbf{H}_s^T\right\} \tag{3.11}$$

The reduced size matrix can then be used to determine the weight matrix $\mathbf{W}$ as:

$$\mathbf{W}^{(s)} = \mathbf{R}_{HH}^{(s)}\left(\mathbf{R}_{HH}^{(s)} + \beta^2 I\right)^{-1} \tag{3.12}$$

The channel prediction matrix is then given by:

$$\hat{\mathbf{H}}_{mmse} = \mathbf{W}^{(s)}\mathbf{H}_s \tag{3.13}$$

3.2.4 ITERATIVE MATRIX INVERSION

The complexity of matrix inversion can be simplified through an iterative process. This section outlines an iterative algorithm which reduces complexity by using only multiplication and addition processes to determine the matrix inverse. The matrix to be inverted is defined as:

$$\mathbf{A} = (\mathbf{R}_{HH} + \beta^2 \mathbf{I})^{-1} \tag{3.14}$$

The iterative matrix inversion method in [84] is modified by introducing a time variant step size μ_k at each iteration. For an $m \times n$ matrix:

For $m \geq n$:

$$\mathbf{W}_{k+1} = \mu_k \mathbf{W}_k + \mathbf{Y}_n(\mathbf{A}^T - \mathbf{B}\mathbf{W}_k) \tag{3.15}$$

where,

$$\mathbf{Y}_n = (\mathbf{I}_n + \mathbf{B}^2)^{-1} \tag{3.16}$$

and,

$$\mathbf{B} = (\mathbf{A}^T\mathbf{A})^2 \tag{3.17}$$

The iteration algorithm is then as follows:

Given an initial matrix $\mathbf{W}_0$ and $\varepsilon > 0$,

if $\|\mathbf{A}^T - \mathbf{B}\mathbf{Y}_{k+1}\|_F^2 \leq \varepsilon$, then output $\mathbf{W}_{k+1}$ else increment k and go back to (3.15).

For $m < n$,

$$\mathbf{W}_{k+1} = \mu_k\mathbf{W}_k + \mathbf{Y}_n(\mathbf{A}^T - \mathbf{C}\mathbf{W}_k) \tag{3.18}$$

where,

$$\mathbf{Y}_m = (\mathbf{I}_m + \mathbf{C}^2)^{-1} \tag{3.19}$$

and,

$$\mathbf{C} = (\mathbf{A}\mathbf{A}^T)^2 \tag{3.20}$$

The iteration algorithm is then as follows:

Given an initial matrix $\mathbf{W}_0$ and $\varepsilon > 0$,

if $\|\mathbf{A}^T - \mathbf{C}\mathbf{Y}_{k+1}\|_F^2 \leq \varepsilon$, then output $\mathbf{W}_{k+1}$ else increment k and go back to (3.18). Only a few iterations are required to achieve a sufficient approximation of the matrix inverse compared to the process required to obtain the exact value.

3.3 CHANNEL PREDICTION FOR FAST FADING

In a fast fading radio channel, the coherence time of the channel has a duration whose length is smaller than one LTE subframe of 1 ms. The fast fading channel is also doubly dispersive in nature [74] and thus the prediction model of section **??** which assumes a flat fading profile is inadequate for this channel. Fast fading causes rapid variation in the CSI and this can lead to rapid loss of capacity due to channel aging. The prediction algorithm developed to increase capacity for fast fading channels is discussed in this section.

In this chapter, a novel 3D-MMSE channel prediction technique is derived. To reduce the complexity of the 3D-MMSE algorithm, three separate prediction filters are used corresponding to the temporal, spatial and frequency correlations.

3.3.1 SYSTEM MODEL

The time domain impulse response of a wireless channel is expressed as:

$$h = \sum_{k=1}^{L} a_k(t)\delta(\tau - \tau_k) \tag{3.21}$$

where τ_k is the delay of the k^{th} path, L is the number of paths and a_k is the complex amplitude. The channel frequency response is determined by taking the Fourier transform of the CIR with respect to the delay can be expressed as:

$$H = \sum_{k=1}^{L} a_k(t) \exp^{-j2\pi f \tau_k} \tag{3.22}$$

The complex amplitude a_k can be expressed as:

$$a_k(t) = \alpha_k \exp^{j(2\pi f_k t + \Phi_k)} \tag{3.23}$$

where α_k is the path loss, f_k is the Doppler frequency shift,Φ_k is the phase offset of the k^{th} multipath component respectively.

Consider a SISO channel with K_{fr} subcarriers and K_{tr} OFDM symbols. The double dispersive channel is characterized by multipath delay spread which causes time dispersion and Doppler spread which leads to frequency dispersion. This essentially creates frequency and time selective fading. The transmitted signal consists of a vector

containing K_{tr} OFDM symbols:

$$\mathbf{X}(i,j) = \left[\mathbf{x}_1^T \mathbf{x}_2^T \cdots \mathbf{x}_{K_{tr}}^T\right] \tag{3.24}$$

The i^{th} symbol is in represented by a K_{fr} length vector given by:

$$\mathbf{x}_i = \left[x_{i,1} x_{i,2} \cdots x_{i,K_{tr}}\right] \tag{3.25}$$

The elements $x_{i,j}$ correspond to the i^{th} OFDM symbol on the j^{th} subcarrier where $i \in \{1 \cdots K_{tr}\}$ and $j \in \{1 \cdots K_{fr}\}$. The received vector is given by:

$$\mathbf{Y}(i,j) = \mathbf{H}(i,j)\mathbf{X}(i,j) + \mathbf{Z}(i,j) \tag{3.26}$$

where $\mathbf{H}$ is the $K_{fr} \times K_{tr}$ channel matrix representing the frequency response of the channel with elements in 3.22 and is given by:

$$\mathbf{H}(i,j) = \begin{bmatrix} H_{11} & . & . & . & H_{1K_{tr}} \\ . & . & & & . \\ . & & . & & . \\ . & & & . & . \\ H_{K_{fr}1} & . & . & . & H_{K_{fr}K_{tr}} \end{bmatrix} \tag{3.27}$$

and Z is the AWGN with a variance of β^2. The elements $H_{i,j}$ represent the frequency response of the CIR at the i^{th} OFDM symbol time on the j^{th} subcarrier.

Consider a MIMO system with N_{tx} transmitter antennas and N_{rx}. The channel matrix

can then be expressed as:

$$\mathbf{H} = \begin{bmatrix} \mathbf{H}_{1,1}(i,j) & . & . & . & \mathbf{H}_{1,N_{tx}}(i,j) \\ . & . & & & . \\ . & & . & & . \\ . & & & . & . \\ \mathbf{H}_{N_{rx},1}(i,j) & . & . & . & \mathbf{H}_{N_{rx},N_{tx}}(i,j) \end{bmatrix} \tag{3.28}$$

3.3.2 SPATIAL-TEMPORAL CORRELATIONS

Let $\mathbf{H}_{ij}$ denote the frequency response of the channel between the transmitter antenna m and the receiver antenna n. The spatial-temporal correlation between two channel coefficients for a time interval Δt is expressed as:

$$\rho_{st} = \mathbb{E}\left\{ \frac{\mathbf{H}_{i_1 j_1}(t)\mathbf{H}^H_{i_2 j_2}(t+\Delta t)}{\sqrt{\left|\mathbf{H}_{i_1 j_1}(t)\right|^2 \left|\mathbf{H}_{i_2 j_2}(t)\right|^2}} \right\} \tag{3.29}$$

3.3.3 SPATIAL CORRELATION

The cross-correlation coefficient for two transmitter antennas i_1 and i_2 can be expressed as:

$$\rho^{tx}_{i_1 i_2} = \left\langle \left|\mathbf{H}_{i_1 j}\right|^2, \left|\mathbf{H}_{i_2 j}\right|^2 \right\rangle \tag{3.30}$$

while that of two receiver antennas is:

$$\rho^{rx}_{j_1 j_2} = \left\langle \left|\mathbf{H}_{i j_1}\right|^2, \left|\mathbf{H}_{i j_2}\right|^2 \right\rangle \tag{3.31}$$

The spatial correlation matrices for the transmitter and receiver antennas are defined as:

$$\mathbf{R}_{tx} = \begin{bmatrix} \rho^{tx}_{1,1} & \cdot & \cdot & \cdot & \rho^{tx}_{1,N_{tx}} \\ \cdot & \cdot & & & \cdot \\ \cdot & & \cdot & & \cdot \\ \cdot & & & \cdot & \cdot \\ \rho^{tx}_{N_{tx},1} & \cdot & \cdot & \cdot & \rho^{tx}_{N_{tx},N_{tx}} \end{bmatrix} \tag{3.32}$$

and,

$$\mathbf{R}_{rx} = \begin{bmatrix} \rho^{rx}_{1,1} & \cdot & \cdot & \cdot & \rho^{rx}_{1,N_{rx}} \\ \cdot & \cdot & & & \cdot \\ \cdot & & \cdot & & \cdot \\ \cdot & & & \cdot & \cdot \\ \rho^{rx}_{N_{rx},1} & \cdot & \cdot & \cdot & \rho^{rx}_{N_{rx},N_{rx}} \end{bmatrix} \tag{3.33}$$

The spatial correlation matrix is given by [70]:

$$\mathbf{R}_s = \mathbf{R}_{tx} \otimes \mathbf{R}_{rx} \tag{3.34}$$

3.3.4 TEMPORAL CORRELATIONS

The temporal correlation function can be obtained as:

$$\rho_t(\Delta t) = \rho_{st} \Big| d_r = d_t = 0 \tag{3.35}$$

$$\rho_t(\Delta t) = \sum_{p=1}^{P} \mathbb{E}\left\{ e^{jk(v_{p,q}\Delta t)} \right\} \tag{3.36}$$

The temporal correlation function is dependent on the Doppler shifts and the time interval.

3.3.5 FREQUENCY CORRELATIONS

The frequency correlation function can be determined from the average power delay profile as:

$$\rho_f = \frac{\sum_{p=1}^{P} a_p e^{-j2\pi\tau_p\Delta_f}}{\sum_{p=1}^{P} a_p} \tag{3.37}$$

where Δf is the frequency spacing.

3.3.6 3D MMSE CHANNEL PREDICTION

A 3D MMSE filter is used to exploit the frequency correlations between different subcarriers, the temporal correlation between adjacent subframes and the spatial correlations between different antennas.

Let us denote the matrix of M current and past estimates of the MIMO channel as:

$$\mathcal{H} = \left[\hat{\mathbf{H}}_n \hat{\mathbf{H}}_{n-1} \cdots \hat{\mathbf{H}}_{n-M+1}\right] \tag{3.38}$$

An M-tap filter is used to predict the MIMO channel matrix as $\tilde{\mathbf{H}}_{n+D} = \mathbf{W}_{3D}\mathcal{H}$. The MIMO channel $\hat{\mathbf{H}}_{n+D}$ is predicted using an MMSE filter as $\tilde{\mathbf{H}}_{n+D} = \mathbf{W}_{3D}\hat{\mathbf{H}}$, where $\mathbf{W}_{3D}$ is the frequency time spatial weight matrix for the MMSE filter given by:

$$\mathbf{W}_{3D} = \underset{w}{\operatorname{argmin}}\, \mathbb{E}\left\{ \left\| \mathbf{H}_{n+D} - \hat{\mathbf{H}}_{n+D} \right\|^2 \right\} \tag{3.39}$$

From the orthogonality principle,

$$\mathbb{E}\left\{ \left(\mathbf{H}_{n+D} - \hat{\mathbf{H}}_{n+D} \right) \mathbf{H}_{n+D}^H \right\} = 0 \tag{3.40}$$

The 3D channel prediction filter weight matrix can be expressed as [71]:

$$\mathbf{W}_{3D} = \left(\mathbf{r}_t^T \otimes \mathbf{R}_s\right)\left(\mathbf{R}_t^T \otimes \mathbf{R}_s + \mathbf{R}_v\right)^{-1} \tag{3.41}$$

where $\mathbf{R}_v = (\sigma_n^2 + \sigma_{ICI}^2)\mathbf{I}$. The ICI variance σ_{ICI}^2 is given by [85]:

$$\sigma_{ICI}^2 = \int_{-1}^{1} (1-|x|) J_0(\omega_D T_S x) dx \tag{3.42}$$

where J_0 is the zeroth order Bessel function of the first kind, ω_D is the radian Doppler frequency, T_S is the OFDM symbol time.

The MMSE is given by:

$$\varepsilon_r = r_t(0) - \left(\mathbf{r}_t^T \otimes \mathbf{R}_s\right)\left(\mathbf{R}_t^T \otimes \mathbf{R}_s + \mathbf{R}_v\right)^{-1}\left(\mathbf{r}_t \otimes \mathbf{R}_s\right)^H \tag{3.43}$$

The computation of $\mathbf{W}_{3D}$ requires the inversion of a block Toeplitz matrix of size $N \times N$ where $N = \left(N_{tx} N_{rx} K_{fr} K_{tr} M\right)$. Inversion of such a large matrix leads to a high computational complexity with $\mathcal{O}(N^3)$.

3.3.7 ICI CANCELLATION

In a fast fading channel the ICI is significant enough that a mechanism for its estimation and reduction becomes necessary. This is performed through channel equalization at the receiver. Various equalization techniques have been proposed to mitigateICI in channels with high Doppler spread including zero-forcing (ZF), successive interference cancellation (SIC) and MMSE schemes [86–89]. In this research work, the method proposed in [89] is used as the ICI equalization algorithm. The received symbols are divided into reliable and unreliable symbols based on a dynamic threshold. A recursive algorithm is then deployed to cancel the contribution of the subset of symbols with the highest SNR.

3.3.8 APPROXIMATE 3D-MMSE CHANNEL PREDICTION ALGORITHM

The approximate 3D-MMSE prediction technique is proposed to reduce the complexity inherent in the classical MMSE algorithm by the following measures:

(a) Perform the channel prediction using a 3-step technique of separate temporal,frequency and spatial correlation filters.

(b) Reduce the inherent matrix inversion complexity through approximation.

3.3.9 TEMPORAL CORRELATIONS FILTER

To exploit the temporal correlations a correlations filter is introduced, $\tilde{\mathbf{H}}_{ft} = \mathbf{W}_{ft}\mathcal{H}$. The prediction filter weight matrix $\mathbf{W}_{ft}$ is derived from the temporal correlations between subframes and can be expressed as:

$$\mathbf{W}_{ft} = E\left\{\left|\left|\mathbf{H}_{ft} - \mathbf{W}_{ft}^{H}\hat{\mathbf{H}}_{ft}\right|\right|^{2}\right\} \tag{3.44}$$

From to the orthogonality principle,

$$\mathbb{E}\left\{\left(\mathbf{H} - \mathbf{W}_{t}^{H}\hat{\mathbf{H}}_{t}\right)^{*}\hat{\mathbf{H}}_{t}\right\} = 0 \tag{3.45}$$

It can be shown that the weight matrix is given by [71]:

$$\mathbf{W}_{t} = (\mathbf{R}_{t} + \beta^{2}\mathbf{I})^{-1}\mathbf{r}_{t} \tag{3.46}$$

where is the vector of cross correlations.

3.3.10 FREQUENCY CORRELATIONS FILTER

To exploit the correlations between the subcarriers, a frequency correlations filter is applied to the temporal prediction as:

$$\tilde{\mathbf{H}}_{ft} = \mathbf{W}_f \tilde{\mathbf{H}}_t \tag{3.47}$$

According to the orthogonality principle,

$$\mathbb{E}\left\{ \left(\mathbf{H}_{ft} - \mathbf{W}_f^H \tilde{\mathbf{H}_{ft}} \right)^* \tilde{\mathbf{H}}_{ft} \right\} = 0 \tag{3.48}$$

Solving (3.47) and (3.48):

$$\mathbf{W}_f = \mathbf{R}_{h\tilde{h}_t} \mathbf{R}_{\tilde{h}_t}^{-1} \tag{3.49}$$

3.3.11 SPATIAL CORRELATIONS FILTER

To exploit the correlations between the MIMO antennas a spatial correlations filter is applied to the frequency-time prediction as:

$$\tilde{\mathbf{H}}_s = \mathbf{W}_s \tilde{\mathbf{H}}_{ft} \tag{3.50}$$

According to the orthogonality principle,

$$\mathbb{E}\left\{ \left(\mathbf{H}_{ft} - \mathbf{W}_s^H \tilde{\mathbf{H}_{ft}} \right)^* \tilde{\mathbf{H}}_{ft} \right\} = 0 \tag{3.51}$$

Solving (3.50) and (3.51):

$$\mathbf{W}_s = \mathbf{R}_{h\tilde{h}_{ft}} \mathbf{R}_{\tilde{h}_{ft}}^{-1} \tag{3.52}$$

where $\mathbf{R}_{h\tilde{h}_{ft}}$ is the cross-correlation matrix given by:

$$\begin{aligned}\mathbf{R}_{h\tilde{h}_{ft}} &= \mathbb{E}\left\{\mathbf{H}_{ft}\tilde{\mathbf{H}}_{ft}^{H}\right\} \\ &= \mathbf{r}_{ft}^{H}\mathbf{W}_{ft}\mathbf{R}_{s}\end{aligned}$$

and $\mathbf{R}_{\tilde{h}_{ft}}$ is the autocorrelation matrix expressed as:

$$\begin{aligned}\mathbf{R}_{\tilde{h}_{ft}} &= \mathbb{E}\left\{\tilde{\mathbf{H}}_{ft}\tilde{\mathbf{H}}_{t}^{H}\right\} \\ &= (\mathbf{W}_{ft}^{H}\mathbf{R}_{\mathbf{t}}\mathbf{W}_{ft})\mathbf{R}_{s} + (\mathbf{W}_{ft}\mathbf{W}_{ft}^{H})\beta^{2}\mathbf{I}\end{aligned}$$

CHAPTER FOUR

RESULTS AND ANALYSIS

In this chapter, a broad overview of the simulation model is presented as well as the tools and configuration parameters. Next is a presentation and analysis of the simulation results, first for the block fading channel and then for the fast fading channel.

4.1 SIMULATION MODEL

In this research work, the simulation scenario consists of the LTE downlink of a single cell consisting of a single eNB and a finite set of arbitrarily numbered mobile users in a MIMO configuration. The main tools used were MATLAB vR2015a and an LTE link level simulator for MATLAB in which the LTE physical layer is abstracted by simplified models as set out in [90]. The simulator consists of three main components: the transmitter, receiver and the channel model each of which is implemented in MATLAB code. As shown in Figure 4.1, the transmitter and receiver are linked via a channel model.

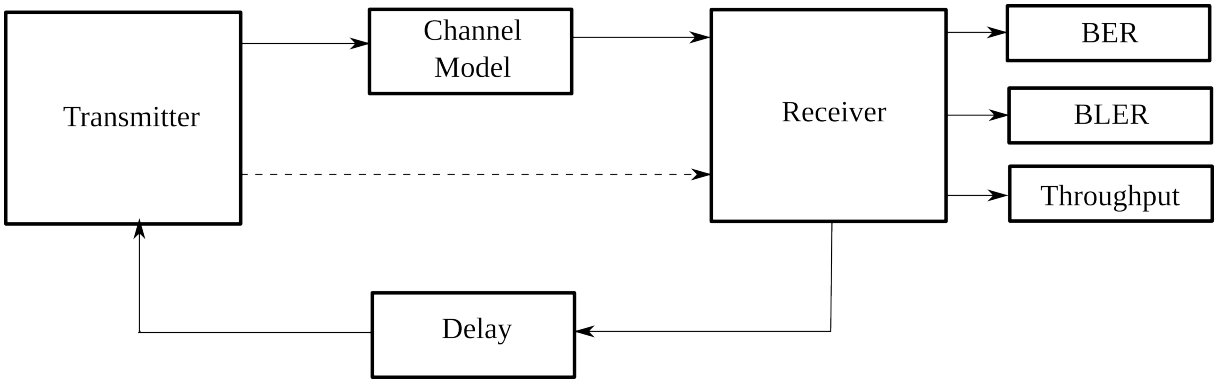

Fig. 4.1 Simulator Structure

4.1.1 TRANSMITTER MODEL

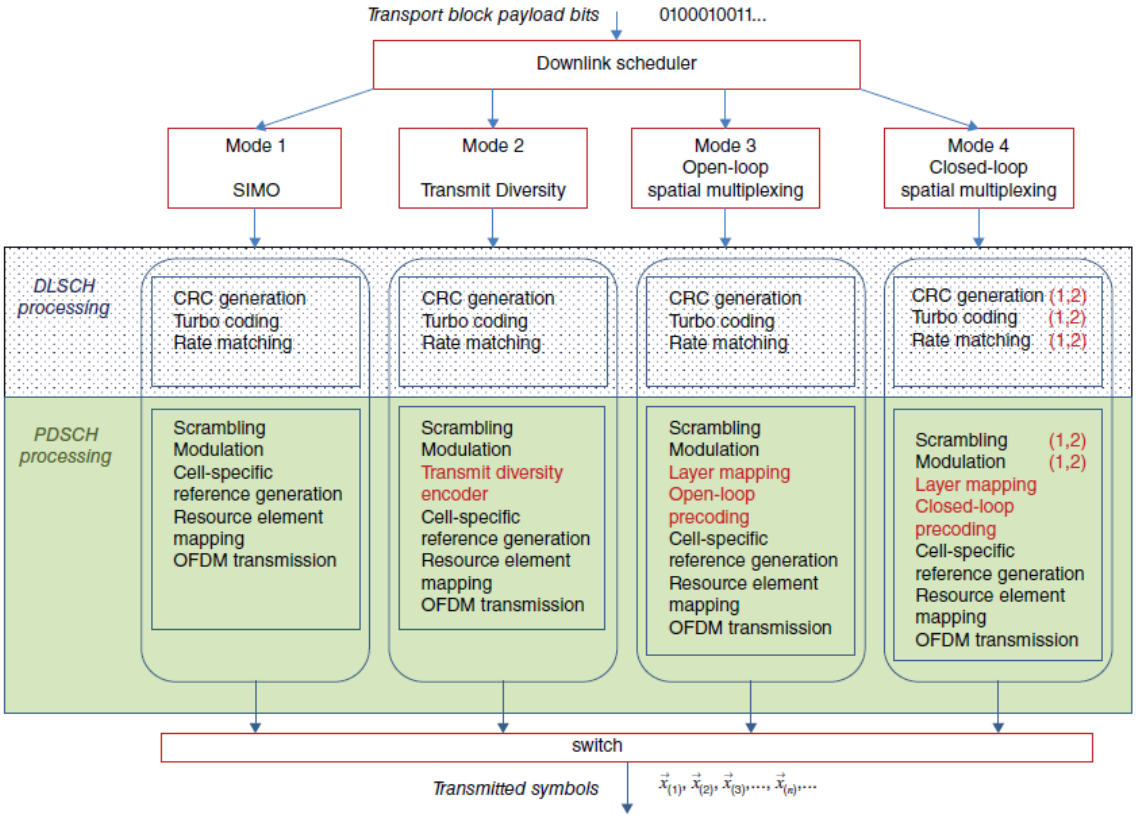

Fig. 4.2 Transmitter Structure

In the transmitter, the signal processing is applied to the data bits provided by the transport channel. In each LTE subframe, the scheduler selects one of the four possible MIMO modes with the selected mode depending on the feedback parameters sent by the receiver. Figure 4.2 shows the transmitter model with the various processing operations implemented through different MATLAB scripts. These operations form part of the Downlink Shared Channel (DLSCH) and Physical Downlink Shared Channel (PDLSCH) processing steps.

4.1.2 CHANNEL MODEL

The channel model used in the simulator is the WINNER MATLAB implementation [91].

4.1.3 RECEIVER MODEL

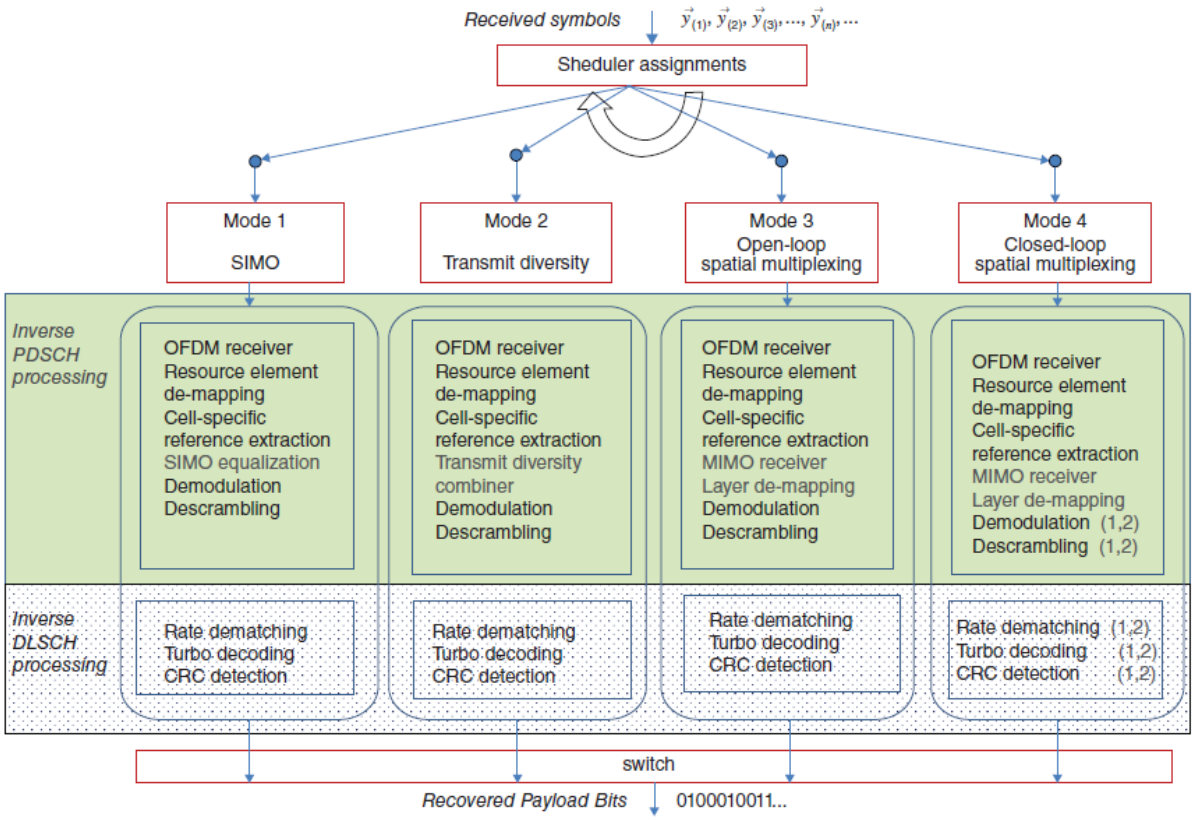

Fig. 4.3 Receiver Structure

At the receiver, the signal processing operations are applied to the received symbols. Figure 4.3 shows the receiver model with the various processing operations implemented through MATLAB scripts. The initial receiver operations are independent of the MIMO mode. These include the resource element demapping, CSR extraction and OFDM receiver. The resource grid is then reconstructed and from the pilot symbols, the channel estimate is computed.

4.1.4 SIMULATION METRICS

For the simulation, the MSE and the average sum capacity or throughput are plotted for various values of feedback delay whose selected range is 0 - 15 ms, this range is selected in order to be within the typical delay value of 8 ms for the LTE downlink. To study the effect of the Doppler spread, the simulation is repeated for Doppler spread values of 10,100 and 200 Hz for both the MSE and the average capacity. In order to ensure that the simulations reflect the long term channel state, the MSE and capacity are tracked over 10,000 LTE subframes.

4.2 PERFORMANCE ANALYSIS FOR BLOCK FADING CHANNELS

The scenario simulated is an LTE downlink system with a carrier frequency of 2.0 GHz, a bandwidth of 5 MHz subdivided into 25 RBs or 300 subcarriers. The simulation parameters are summarized in table 4.1. The LTE downlink is simulated with optimal rate, power and subcarrier allocation in order to isolate the effects of the channel prediction. For comparative analysis purposes the real channel state, called perfect predictor are included in the results. A comparative analysis of the proposed algorithm vis-à-vis the RLS, Normalised Linear Mean Square (NLMS) and MMSE algorithms is then performed.

Table 4.1 Simulation Parameters for Block Fading Channel

Parameter Name	**Value**
Transmission Mode	Closed Loop Spatial Multiplexing
MIMO Configuration	4 x 2
Bandwidth	5 MHz
Subcarriers	300
Channel Model	WINNER II
Feedback Delay	0 - 15 ms
Frequency	2.3 GHz
Doppler Spread	0 - 100 Hz
Number of Paths	8
Channel Estimation	Ideal

4.2.1 VARIATION OF MSE WITH DELAY FOR BLOCK FADING

In this section, the results which show the variation of the MSE with feedback delay and the Doppler spread of the channel are presented. The delay is varied from 0 ms to 15 ms. The prediction MSE is then averaged for 10000 subframes. For each of the predictors, a plot of the MSE vs the feedback delay at Doppler spread values of $f_d = 10$ Hz, 100 Hz is shown.

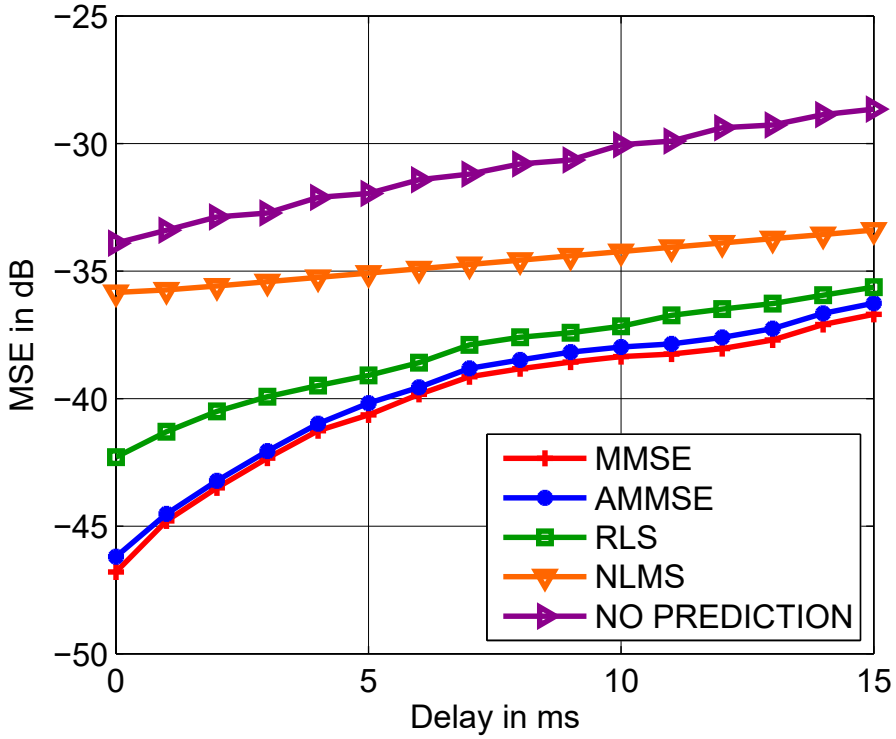

Fig. 4.4 Block Fading MSE v Delay at 10 Hz Doppler spread

In Figure 4.4, the feedback delay is varied between 0 ms and 15 ms while the Doppler spread is fixed at 10 Hz corresponding to a slow fading channel. All prediction algorithms exhibit low MSE values -35 dB to -47 dB compared with the no prediction scenario. This is because for slow fading channels, there is high correlation between adjacent subframes used in the prediction computation which means there is only a small difference between the predicted channel and the actual channel state. It can be seen that the MSE increases with rising delay values for all the prediction algorithms. This is expected behavior since prediction becomes more difficult many steps into the future. It can also be noted that the RLS and approximate MMSE algorithms have a performance that is close to that of the full complexity MMSE algorithm with a performance degradation of about 0.2 dB.

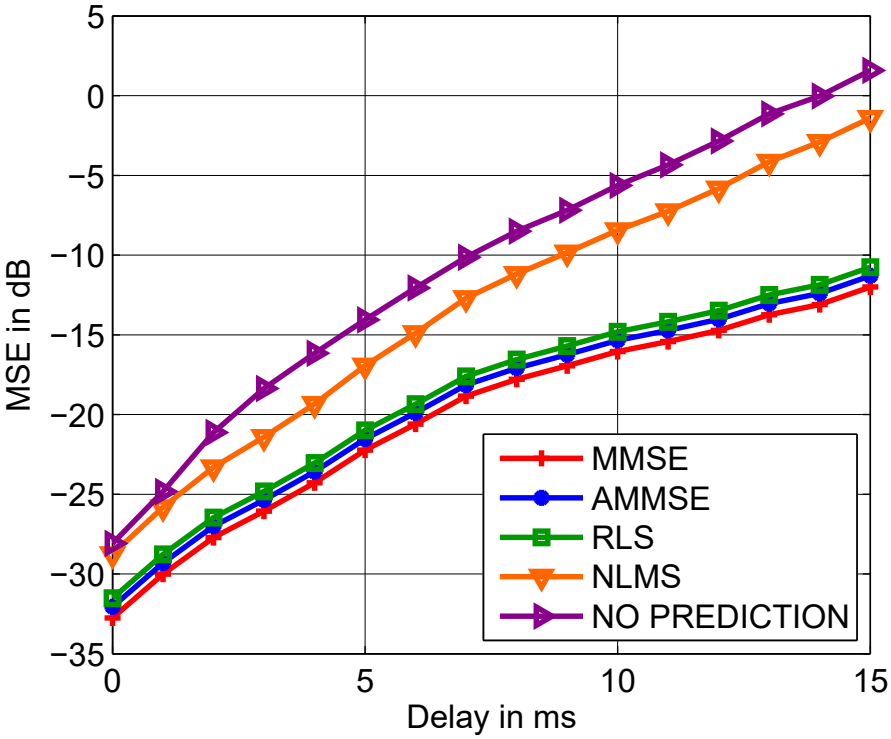

Fig. 4.5 Block Fading MSE v Delay at 100 Hz Doppler spread

In Figure 4.5, the feedback delay is varied between 0 ms and 15 ms while the Maximum Doppler Shift is fixed at 100 Hz corresponding to a faster fading channel. It can be seen that the MSE increases with Doppler spread for all the prediction algorithms. The MSE values are much higher compared with the slow fading channels of Figure 4.4. This is due to the fact that as the Doppler spread increases, the temporal correlations decrease leading to an increase in the difference between the actual and the predicted channel state and thus a higher MSE.

4.2.2 VARIATION OF MSE WITH DOPPLER SPREAD FOR BLOCK FADING

In this section, the results which show the variation of the MSE with the Doppler spread of the block fading channel are shown.

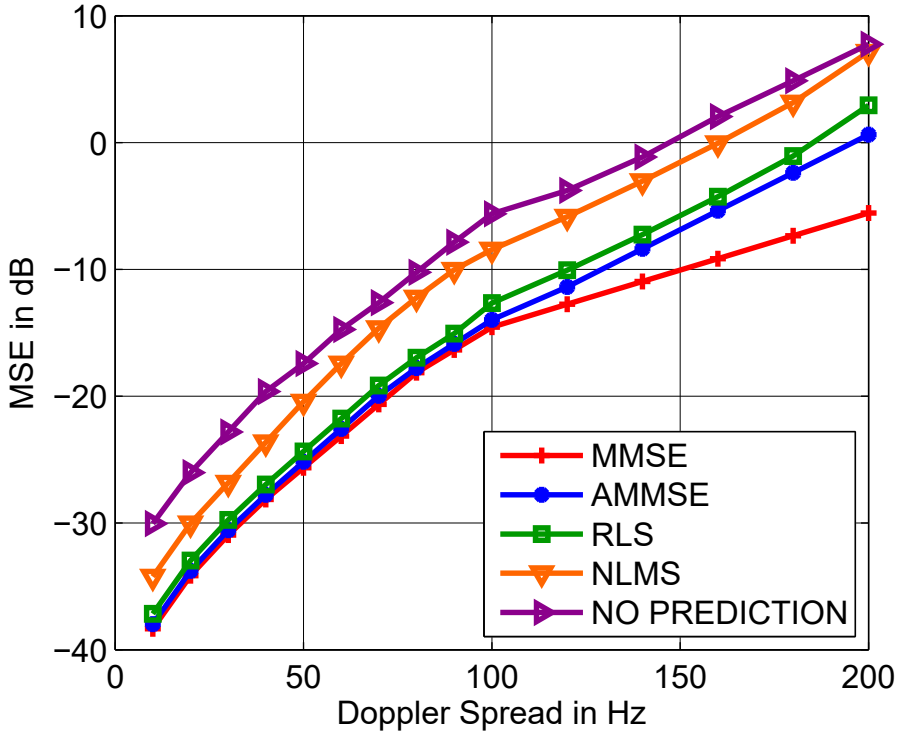

Fig. 4.6 Block Fading MSE v Doppler spread at delay = 10 ms

In Figure 4.6, the Doppler spread is varied between 0 Hz to 200 Hz while the feedback delay is fixed at 10 ms. The MSE for the approximate MMSE remain within 2.8 dB compared to that of the MMSE for Doppler spread values of 100 Hz. At higher maximum Doppler shifts, the Approximate Minimum Mean Square Error (AMMSE) algorithm shows increasing deviation from the classical MMSE algorithm. This is because the core technique used of matrix sampling instead of the use of the full autocorrelation matrix in the computations results in loss of accuracy in the predicted channel.

4.2.3 VARIATION OF THROUGHPUT WITH DELAY FOR BLOCK FADING

In this section, the results which show the variation of the average system capacity (i.e. the time average of the throughput) with feedback delay and the Doppler spread of the channel are presented. The delay is varied from 0 ms to 15 ms. For each of the

predictors, a plot of the throughput vs the feedback delay at Doppler spread values of $f_d = 10$ Hz, 100 Hz is shown.

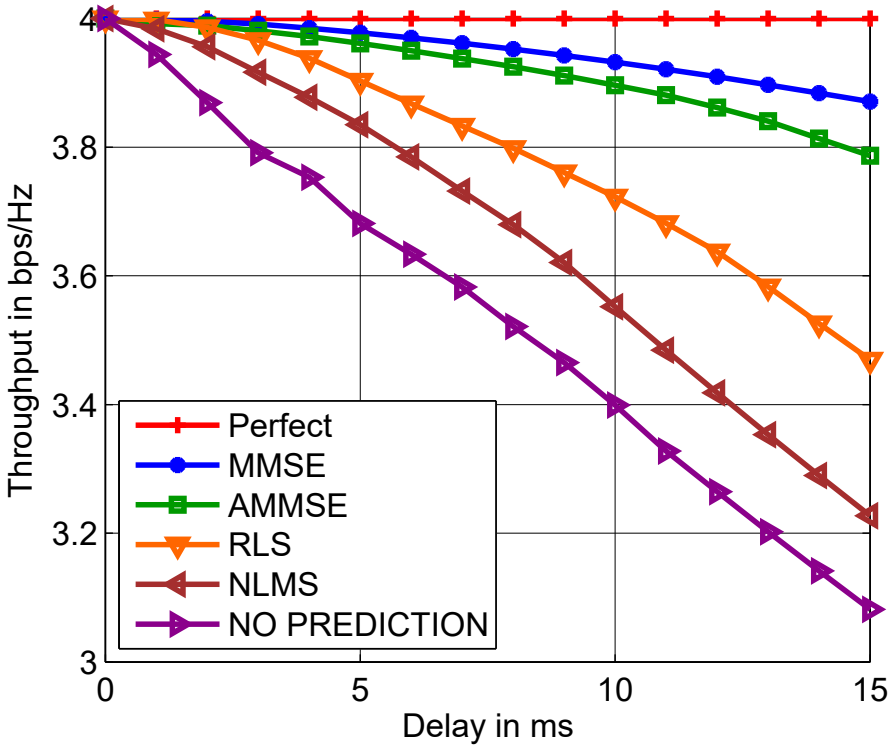

Fig. 4.7 Block Fading Throughput v Delay at 10 Hz Doppler spread

In Figure 4.7, the average sum capacity of the LTE system is plotted for the different algorithms as a function of the feedback delay. The Doppler spread is fixed at 10 Hz. For all predictors, there is a slight improvement in capacity compared to the case without prediction ranging from 3.8% for the NLMS algorithm to 4.9% for the MMSE algorithm. These relatively limited gains are due to the fact that at the low Doppler spread values the channel is relatively constant and prediction offers only limited value.

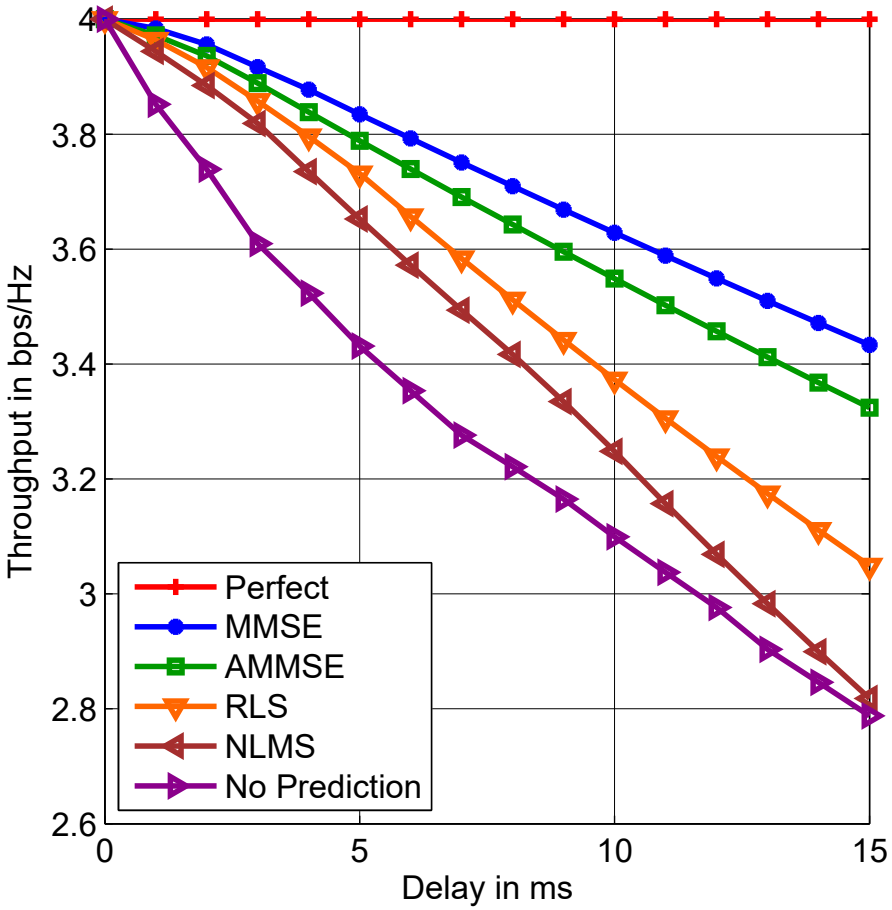

Fig. 4.8 Block Fading Throughput v Delay at 100 Hz Doppler spread

Figure 4.8 depicts a scenario in which the Doppler spread is set at 100 Hz. At this Doppler spread value, the AMMSE and MMSE prediction methods provide 10.8% and 11.7% throughput performance gain at 5 ms feedback delay and 20.2% and 21.6% gain at 10 ms delay compared to the case without prediction. These gains are the result of exploiting the high temporal correlations and illustrate the benefits of channel prediction to combat channel aging. In addition, the throughput is lower for all predictors when the Doppler spread value is raised from 10 Hz to 100 Hz. This is not surprising because at a higher Doppler spread, the channel variation is faster and the prediction algorithm experiences larger MSE thereby causing improper link adaptation.

4.2.4 BLOCK FADING CHANNEL PREDICTION ALGORITHMS COMPLEXITY ANALYSIS

The complexities of the prediction algorithms algorithms are compared using the big O notation [92] and have been outlined in Table 4.2 where $\mathbb{N} = K \times N_T \times N_R$,K is the number of subcarriers,N_T is the number of transmitting antennas, N_R is the number of receiver antennas, M is the prediction filter memory and L is the down-sampling factor. The simulation parameters used were $K = 25$, $N_T = 4$, $N_R = 2$, $M = 8$ and $L = 4$.

Table 4.2 Complexity of M-order MIMO channel prediction algorithms

Algorithm	**Design**	**Prediction**	**Update**
MMSE	$\mathcal{O}(\mathbb{N}^3M^3)$	$\mathcal{O}(\mathbb{N}^2M)$	-
AMMSE	$\mathcal{O}((\mathbb{N}/L)^3M^3)$	$\mathcal{O}((\mathbb{N}/L)^2M)$	-
NLMS	-	$\mathcal{O}(\mathbb{N}\log_2\mathbb{N})$	$\mathcal{O}(M)$
RLS	-	$\mathcal{O}(\mathbb{N}\log_2\mathbb{N})$	$\mathcal{O}(M^2)$

For the chosen simulation parameters, the AMMSE algorithm results in a 88.437% reduction in complexity for the filter design stage which is the most computationally complex stage. The AMMSE algorithm is thus significantly less complex compared to the classical MMSE algorithm. The adaptive channel predictors based on the NLMS and RLS algorithms provide less complexity but at the cost of high MSE values for the NLMS method and high convergence times for the RLS technique. Figure 4.9 is a plot of the MSE v number of iteration for the iteratively computed matrix inverse. The SNR is fixed at 18 dB. An MSE of -46 dB is sufficient to achieve the LTE defined BLER baseline of 10% and the AMMSE achieves this target using less than 100 iterations.

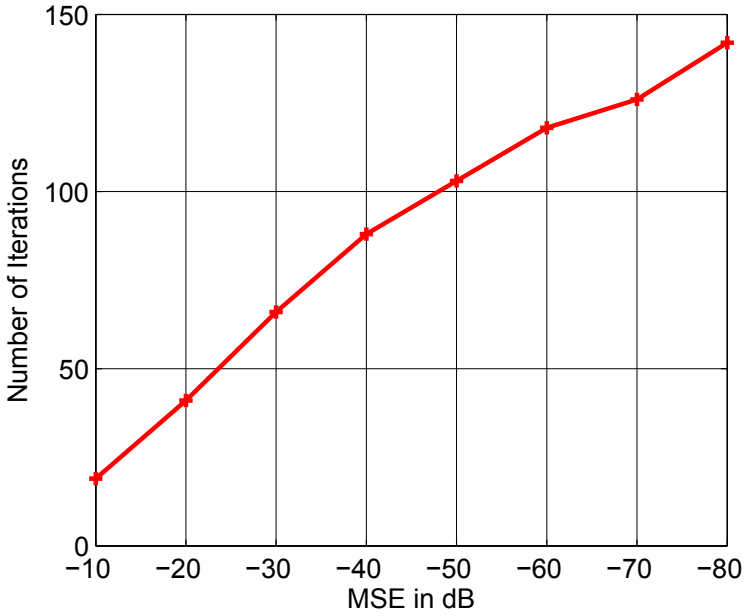

Fig. 4.9 MSE v Number of iterations for approximate matrix inverse

4.3 PERFORMANCE ANALYSIS FOR FAST FADING CHANNELS

An LTE downlink system with a carrier frequency of 2.3 GHz was simulated, a bandwidth of 1.4 MHz subdivided into 6 RBS or 72 subcarriers, using the simulator developed in [90]. The simulation parameters are summarized in Table 4.3. Included is the performance without prediction, denoted as "No Prediction" to act as a baseline. A comparative analysis of the proposed Approximate Three Dimension Minimum Mean Square Error (A3D-MMSE) algorithm vis-à-vis the full complexity Three Dimension Minimum Mean Square Error (3D-MMSE) algorithm is then performed.

Table 4.3 Simulation Parameters for Fast Fading Channel

Parameter Name	**Value**
Transmission Mode	Closed Loop Spatial Multiplexing
MIMO Configuration	2 x 2
Bandwidth	1.4 MHz
Number of Subcarriers	72
Channel Model	WINNER II
Doppler Spread	0 - 200 Hz
Number of Paths	8
Scheduler	Proportional Fair Scheduler
Number of Mobiles	10
Carrier Frequency	2.3 GHz

4.3.1 VARIATION OF MSE WITH DELAY FOR FAST FADING

In this section, the results which show the variation of the mean square error (MSE) v feedback delay of the channel are presented. The delay is varied from 0 ms to 15 ms. The prediction MSE is then averaged for 10000 subframes. For a delay d = 0, the channel predictor becomes a channel estimator similar to [77, 78]. For each of the predictors, the variation of the MSE vs the feedback delay at Doppler spread values of $f_d = 100$ Hz, 200 Hz is plotted.

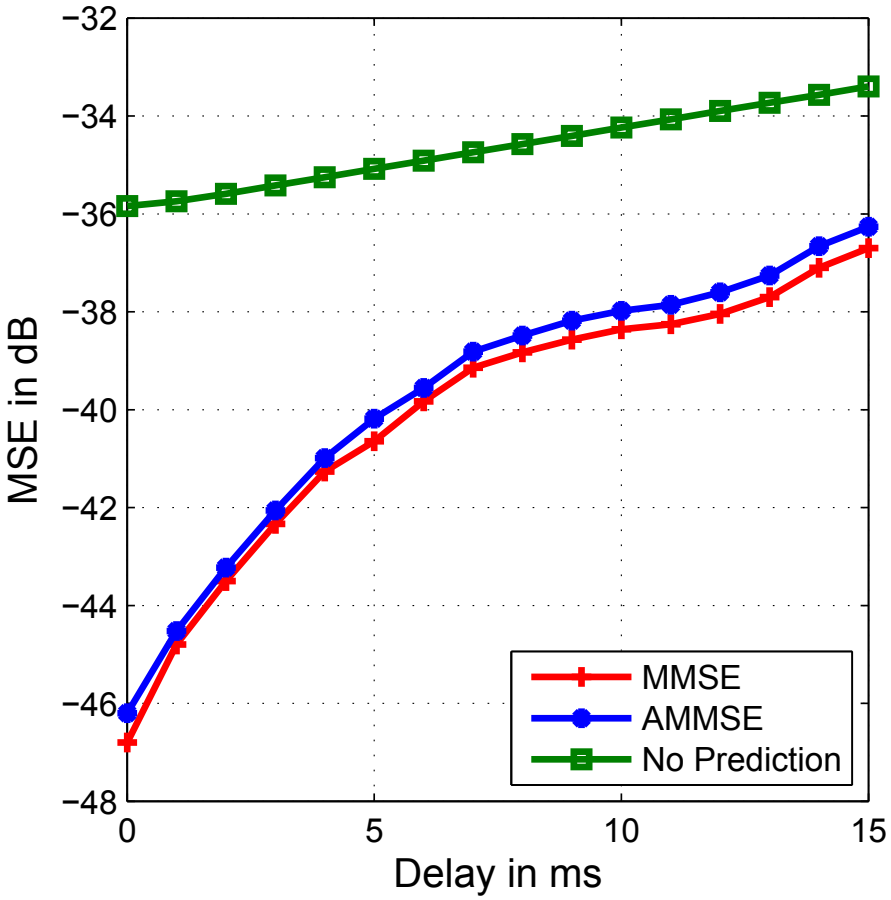

Fig. 4.10 Fast Fading MSE v Delay at 10 Hz Doppler spread

In Figure 4.10, the MSE of the LTE system is plotted for the different algorithms as a function of the feedback delay. The Doppler spread is fixed at 10 Hz corresponding to a slowly varying channel. Both the 3D-MMSE and A3D-MMSE exhibit low MSE values -36 dB to -47 dB compared with the no prediction scenario. This is due to the high temporal correlation between adjacent subframes which means there is only a small difference between the predicted channel and the actual channel state.

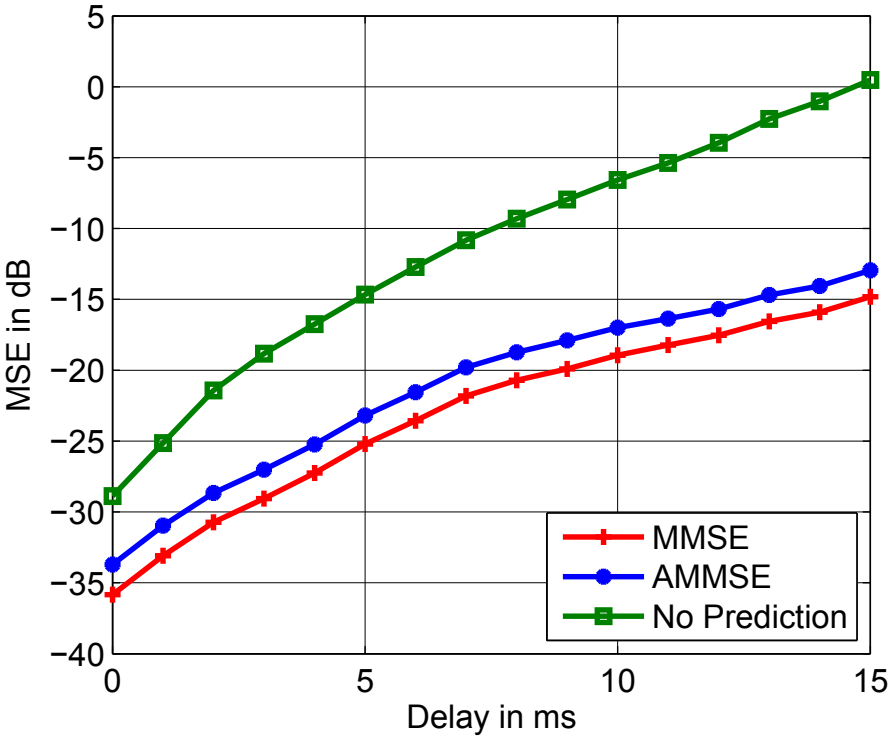

Fig. 4.11 Fast Fading MSE v Delay at 100 Hz Doppler spread

In Figure 4.11, the MSE of the LTE system is plotted for the different algorithms as a function of the feedback delay. The Doppler spread is fixed at 100 Hz corresponding to a moderately fast fading channel. The A3D-MMSE algorithm remains within a range of 2.1 - 2.4 dB compared to the 3D-MMSE in the moderately fast fading fading channels. The MSE without prediction increases rapidly with feedback delay. This is expected behavior which illustrates the effects of channel aging in a fast fading channel.

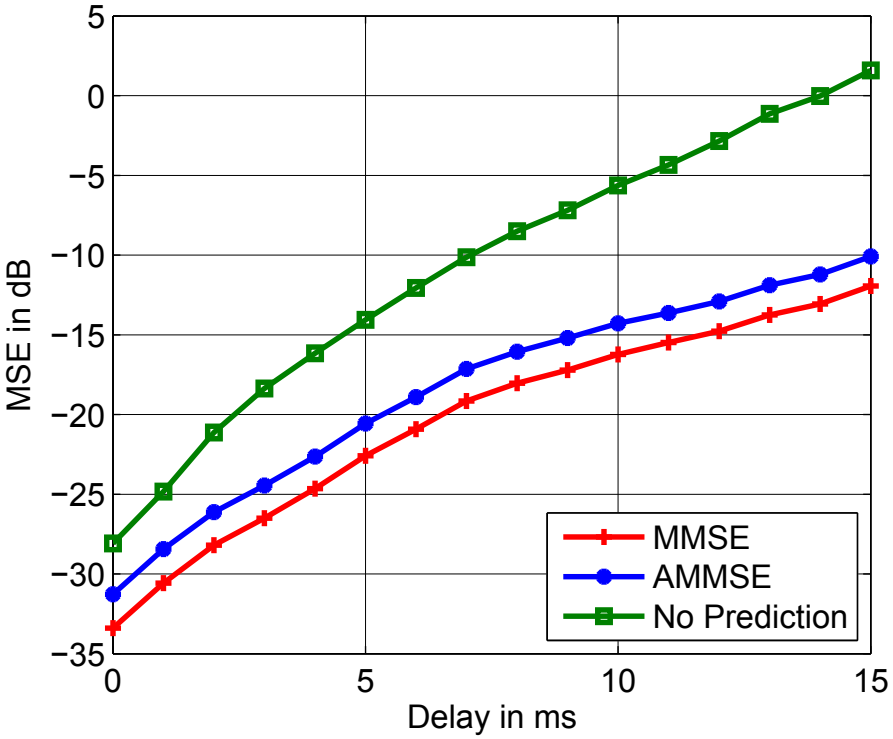

Fig. 4.12 Fast Fading MSE v Delay at 200 Hz Doppler spread

Figure 4.12 depicts a scenario in which the Doppler spread is set at 200 Hz, corresponding to a fast fading channel. It can be seen that the MSE increases with Doppler spread for both the prediction algorithms. The MSE values are much higher compared with the fading channels of Figure 4.11. The main reasons for this observation are twofold; the first is due to the fact that as the Doppler spread increases, the temporal correlations decrease leading to an increase in the difference between the actual and the predicted channel state, in addition, at higher Doppler spread values, the ICI between adjacent subframes becomes more pronounced leading to higher MSE.

4.3.2 VARIATION OF MSE WITH DOPPLER SPREAD FOR FAST FADING

In this section, the results which show the variation of the MSE with the Doppler spread of the fast fading channel are presented. The Doppler spread is varied from $0Hz$ to

200Hz. For each of the predictors, a plot of the MSE vs the Doppler spread at feedback delay values of 10 ms is shown.

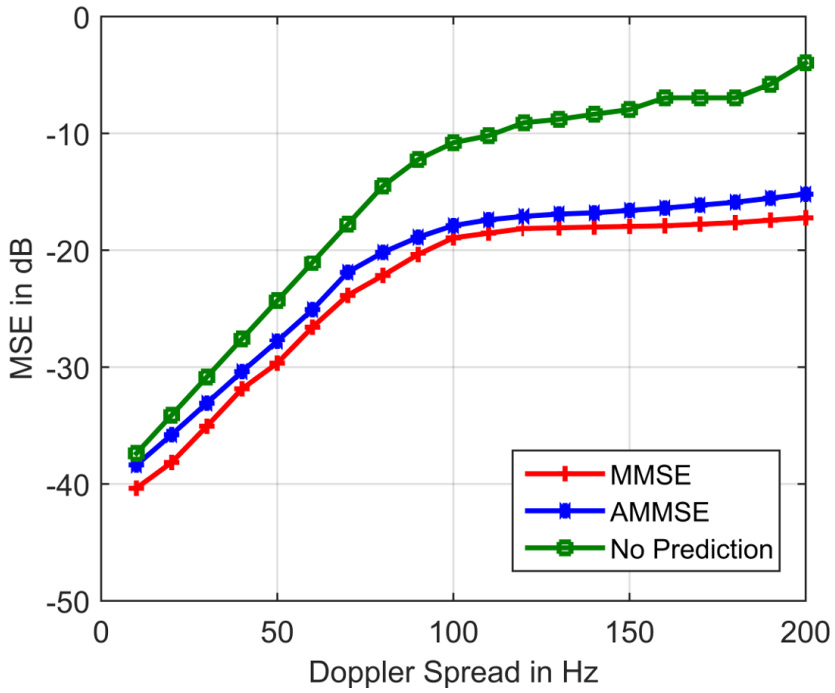

Fig. 4.13 Fast Fading MSE v Doppler spread at delay = 10 ms

In Figure 4.13, the Doppler spread is varied between 0 Hz to 200 Hz while the feedback delay is fixed at 10 ms. The A3D-MMSE algorithm has a poorer performance compared to that of the 3D-MMSE technique with a maximum difference of 2.4 dB between their respective MSE values. This performance decline is because for the 3D-MMSE method, the data used in the prediction is selected adaptively from the temporal, spatial and frequency correlations while in the 3-step A3D-MMSE algorithm, the order is fixed by first exploiting the temporal correlation, followed by the frequency and lastly the spatial correlations thus reducing prediction performance. This degradation in MSE performance for the A3D-MMSE algorithm is an acceptable outcome considering that its achieved at much lower complexity compared to the 3D-MMSE algorithm. Both methods perform much better in comparison with the case without prediction with the

3D-MMSE and A3D-MMSE method providing 12.1 dB and 9.7 db improvement in the MSE respectively.

4.3.3 VARIATION OF THROUGHPUT WITH DELAY FOR FAST FADING

In this section, the results which show the variation of the average system capacity or throughput with feedback delay and the Doppler spread of the channel are presented. For each of the predictors, a plot the throughput vs the feedback delay at Doppler spread values of $f_d = 10$ Hz, 100 Hz, 200 Hz is shown.

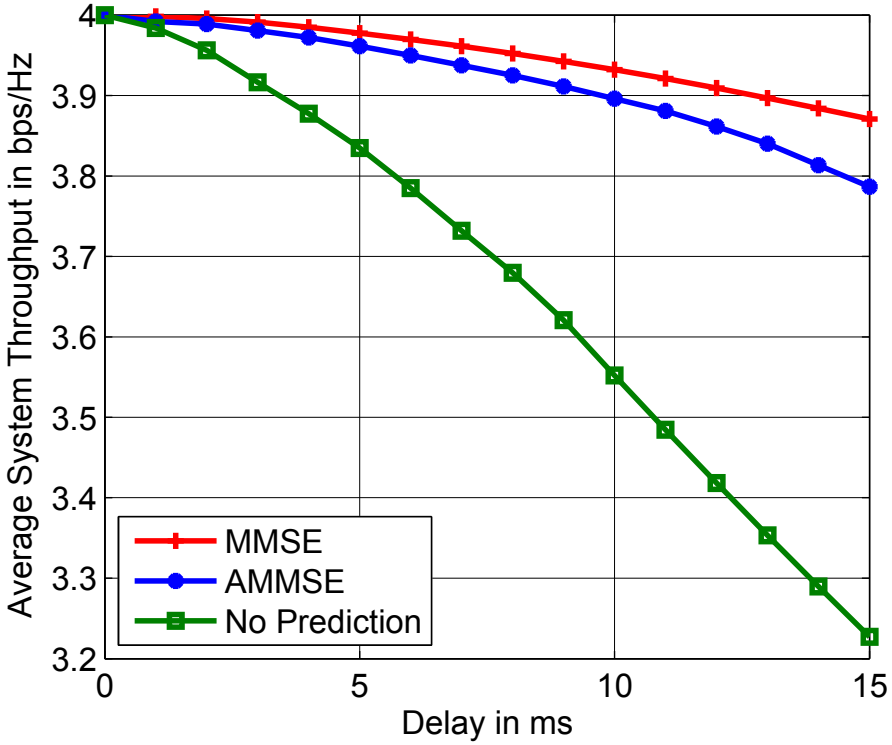

Fig. 4.14 Fast Fading Throughput v Delay at 10 Hz Doppler spread

Figure 4.14 depicts a scenario in which the Doppler spread is set at 10 Hz, corresponding to a slow channel. At this Doppler spread value, the A3D-MMSE and 3D-MMSE prediction methods provide 3.1% and 4.0% throughput performance gain at 5 ms feedback delay compared to the case without prediction. These relatively limited gains are due to the fact that at the low Doppler spread values the channel is

relatively constant and prediction offers only limited value. In Figure 4.15, the average capacity of the LTE system is plotted for the different algorithms as a function of the feedback delay. The Doppler spread is fixed at 100 Hz corresponding to a moderately fast fading channel. At this Doppler spread value, the A3D-MMSE and 3D-MMSE prediction methods provide 10.1% and 10.3% throughput performance gain at 5 ms feedback delay and 20.0% and 20.6% gain at 10 ms delay compared to the case without prediction. These gains are the result of exploiting the high temporal, frequency and spatial correlations and illustrate the benefits of channel prediction when the Doppler spread increases in a channel.

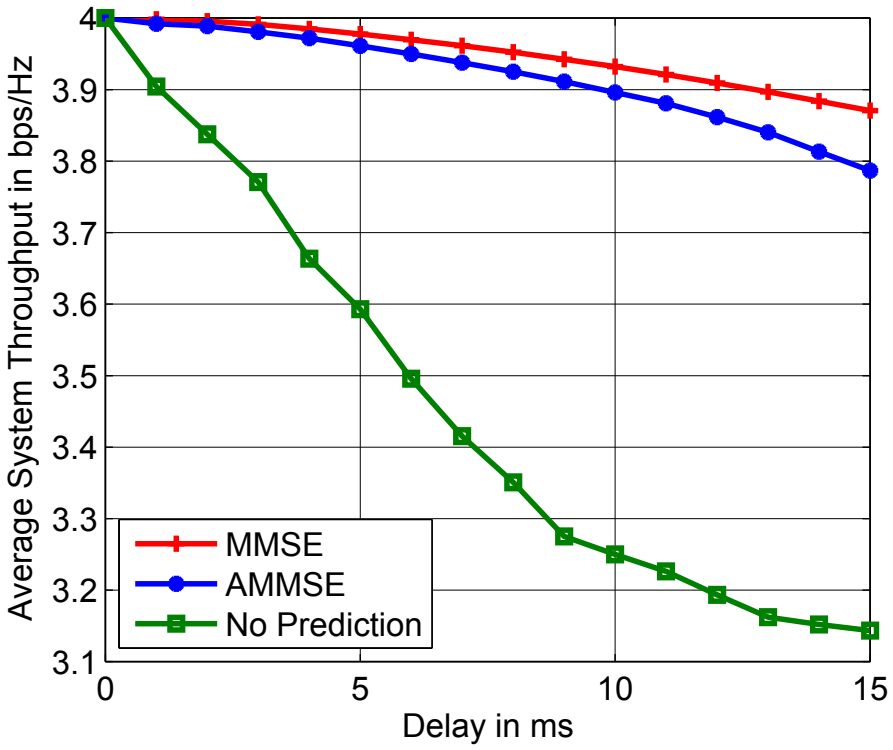

Fig. 4.15 Fast Fading Throughput v Delay at 100 Hz Doppler spread

When the Doppler spread is increased to 200 Hz, corresponding to a speed of 30 m/s, channel prediction becomes increasingly more difficult as the feedback delay increases. Figure 4.16 show the case in which the Doppler spread is set at 200 Hz. It can be observed that as the delay increases, the throughput decreases rapidly. This is due to

the fact that at high Doppler spread, the temporal correlations are low. In addition, the problem of error propagation between successive predictions makes the presented model inadequate for long range fast fading prediction. Error propagation for long range prediction is brought about by the fact that the actual channel estimates are not available at the time of prediction so they are substituted with the imperfect predicted channel realizations.

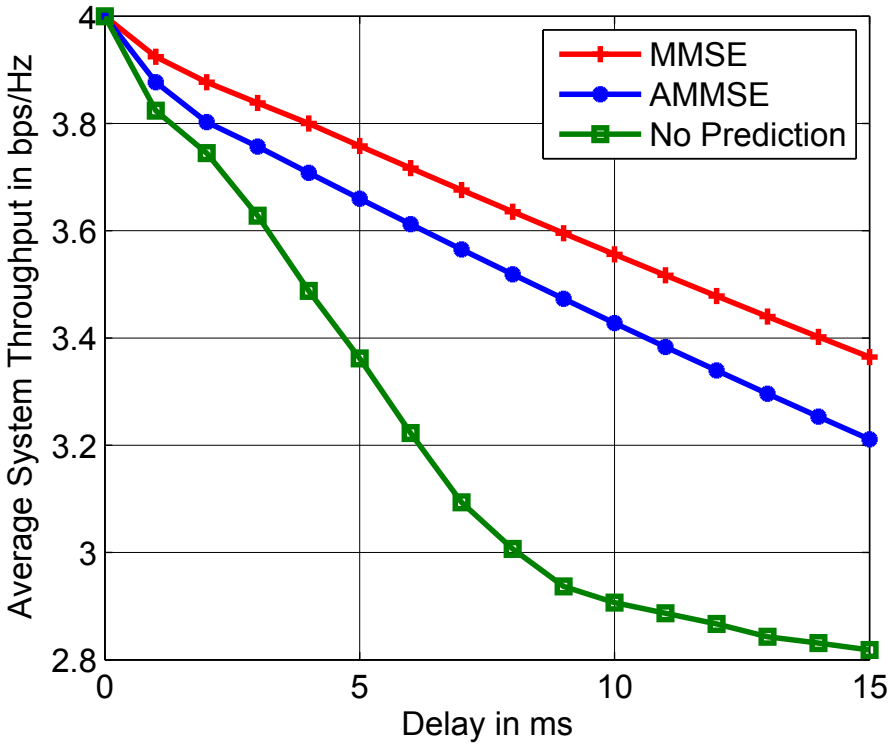

Fig. 4.16 Fast Fading Throughput v Delay at 200 Hz Doppler spread

4.3.4 FAST FADING CHANNEL PREDICTION ALGORITHMS COMPLEXITY ANALYSIS

Table 4.4 Complexity of M-order MIMO fast fading channel prediction algorithms

Algorithm	**Design**	**Prediction**
3D-MMSE	$\mathcal{O}(N^3M^3)$	$\mathcal{O}(N^2M)$
A3D-MMSE	$\mathcal{O}((N/3)^3M^3)$	$\mathcal{O}((N/3)^2M)$

The computational complexities of the prediction algorithms that have been outlined is shown in Table 4.4. The A3D-MMSE is much less complex compared to the full complexity 3D-MMSE algorithm with 11.1% of the complexity for the chosen parameters.

CHAPTER FIVE

CONCLUSION AND FURTHER WORK

5.1 INTRODUCTION

In this chapter, a summary of the most important results from this thesis is presented. Possible further research to extend the current work is also outlined.

5.2 CONCLUSION

The AMMSE channel prediction algorithm is presented as a mechanism for mitigating the effects of channel aging caused by feedback delay in the LTE downlink. In section 3.2 a reduced complexity MMSE prediction algorithm for block fading channels is presented. The results show that channel prediction is important because of its potential to improve performance through compensating for unavoidable feedback and processing delays. For slowly varying channels, the proposed algorithm provides a capacity gain of 3.4% compared to the use of the outdated channel when no prediction is allowed. However, as the Doppler spread increases, the effects of channel aging become more pronounced and the capacity gain from channel prediction rises to 21.6%.

In section 3.3 a three dimensional channel prediction technique is proposed. This is an MMSE based algorithm which utilizes the temporal, frequency and spatial correlation to compute the channel prediction values. The proposed 3D-MMSE algorithm provides a capacity gain of 3.1% for low Doppler spread values rising to 20.6% gain at 100 Hz Doppler spread. However this improvement of the overall system capacity comes at the cost of high complexity. A reduced complexity algorithm is then proposed, the A3D-MMSE predictor which performs the the prediction in a sequence of three steps. The simulation results show that for the studied scenario, the A3D-MMSE has a performance that is nearly the same as that of the full complexity 3D-MMSE algorithm providing 97.1% the capacity gains of the 3D-MMSE method. This degradation in

performance for the A3D-MMSE algorithm is an acceptable outcome considering that its achieved at 11.1% of the complexity of the 3D-MMSE algorithm.

5.3 THESIS CONTRIBUTIONS

The contributions of the thesis can be summarized in two themes as follows: The problem of prediction in a block fading channel is considered and an MMSE channel prediction algorithm is developed.

The framework is then extended to the fast fading scenario where a novel three dimensional MMSE prediction technique is developed. The proposed method exploits the temporal, frequency and spatial correlations in the channel predictor. A three step technique for reducing the high complexity of the MMSE predictor is developed resulting in the A3D-MMSE algorithm.

5.4 FUTURE RESEARCH

A number of issues and challenges still remain to be studied. In this section is a list of possible research topics to build upon the work in this thesis:

In many practical wireless systems, a rich scattering environment is not available especially for large bandwidth systems. The signal is propagated through only a few significant paths and the resulting CIR has a few peaks and many zeros. The channel is therefore described by a sparse matrix which can utilize the compressed sensing technique for channel estimation and prediction. Developing methods for prediction of sparse channels is an interesting research problem.

In the current work, its assumed that each user has a maximum of two antennas. Performance analysis of capacity, detection and feedback techniques for massive MIMO systems with multi-antenna MTs should be studied.

An interesting area of further research is to incorporate the prediction techniques developed in this thesis into Multi-User MIMO systems that require coordinated trans-

missions. The system performance should then be investigated to determine if there is any performance improvement.

REFERENCES

[1] M. K. Simon and M.-S. Alouini, *Digital communication over fading channels*. John Wiley & Sons, 2005, vol. 95.

[2] L. Venturino, N. Prasad, and X. Wang, "Coordinated scheduling and power allocation in downlink multicell OFDMA networks," *Vehicular Technology, IEEE Transactions on*, vol. 58, no. 6, pp. 2835–2848, 2009.

[3] Q. Liu, "Channel prediction for multiuser downlink LTE-TDD systems," in *Personal, Indoor, and Mobile Radio Communications (PIMRC), 2015 IEEE 26th Annual International Symposium on*. IEEE, 2015, pp. 160–165.

[4] A. S. Khrwat, "Channel prediction for limited feedback precoded MIMO-OFDM systems," in *Telecommunications (ICT), 2012 19th International Conference on*. IEEE, 2012, pp. 1–6.

[5] S. Galih, R. Karlina, F. Nugroho, A. Irawan, T. Adiono, and A. Kurniawan, "Low complexity down-sampled MMSE (DMMSE) channel estimation for downlink OFDMA IEEE 802.16e system," in *Microwave, Antenna, Propagation and EMC Technologies for Wireless Communications, 2009 3rd IEEE International Symposium on*, Oct 2009, pp. 273–277.

[6] S. Pietrzyk, *OFDMA for Broadband Wireless Access (Artech House Mobile Communications)*. Artech House, Inc., 2006.

[7] E. Dahlman, S. Parkvall, and J. Skold, *4G: LTE/LTE-advanced for mobile broadband*. Academic press, 2013.

[8] D. Martín-Sacristán, J. F. Monserrat, J. Cabrejas-Peñuelas, D. Calabuig, S. Garrigas, and N. Cardona, "On the way towards fourth-generation mobile: 3GPP LTE and LTE-advanced," *EURASIP Journal on Wireless Communications and Networking*, vol. 2009, p. 4, 2009.

[9] U. Barth, "3GPP Long-Term Evolution/System Architecture Evolution Overview," *Alcatel White Paper*, 2006.

[10] J. Zyren and W. McCoy, "Overview of the 3GPP long term evolution physical layer," *Freescale Semiconductor, Inc., white paper*, 2007.

[11] A. Ghosh, R. Ratasuk, B. Mondal, N. Mangalvedhe, and T. Thomas, "LTE-advanced: next-generation wireless broadband technology [Invited Paper]," *Wireless Communications, IEEE*, vol. 17, no. 3, pp. 10–22, June 2010.

[12] Q. Li, G. Li, W. Lee, M.-i. Lee, D. Mazzarese, B. Clerckx, and Z. Li, "MIMO techniques in WiMAX and LTE: a feature overview," *Communications Magazine, IEEE*, vol. 48, no. 5, pp. 86–92, 2010.

[13] S. Sesia, I. Toufik, and M. Baker, *LTE - The UMTS Long Term Evolution: From Theory to Practice*. Wiley, 2011.

[14] D. Gesbert, H. Bolcskei, D. GORE, and A. Paulraj, "Outdoor MIMO wireless channels: models and performance prediction," *Communications, IEEE Transactions on*, vol. 50, no. 12, pp. 1926–1934, Dec 2002.

[15] Y. S. Cho, J. Kim, W. Y. Yang, and C. G. Kang, *MIMO-OFDM wireless communications with MATLAB*. John Wiley & Sons, 2010.

[16] K. Lee and D. Williams, "A space-frequency transmitter diversity technique for OFDM systems," in *Global Telecommunications Conference, 2000. GLOBECOM '00. IEEE*, vol. 3, 2000, pp. 1473–1477 vol.3.

[17] I. G. Kim, Y. Han, Y. H. Kim, and S. C. Bang, "Transmit diversity and multiplexing methods for 3G-LTE downlink control channels," in *Vehicular Technology Conference, 2006. VTC-2006 Fall. 2006 IEEE 64th*. IEEE, 2006, pp. 1–4.

[18] B. Furht and S. A. Ahson, *Long Term Evolution: 3GPP LTE radio and cellular technology*. CRC Press, 2009.

[19] W. Guo, J. Fan, G. Y. Li, Q. Yin, X. Zhu, and Y. Fu, "3D MIMO with rank adaptation for LTE-A downlink transmission," in *Personal, Indoor, and Mobile Radio Communications (PIMRC), 2015 IEEE 26th Annual International Symposium on*. IEEE, 2015, pp. 517–521.

[20] F. Khan, *LTE for 4G mobile broadband: air interface technologies and performance*. Cambridge University Press, 2009.

[21] S. L. Loyka, "Channel capacity of MIMO architecture using the exponential correlation matrix," *Communications Letters, IEEE*, vol. 5, no. 9, pp. 369–371, 2001.

[22] S. A. Jafar, "Fundamental capacity limits of multiple antenna wireless systems," Ph.D. dissertation, Stanford University, 2003.

[23] M. Kobayashi and G. Caire, "An iterative water-filling algorithm for maximum weighted sum-rate of Gaussian MIMO-BC," *Selected Areas in Communications, IEEE Journal on*, vol. 24, no. 8, pp. 1640–1646, 2006.

[24] P. Almers, E. Bonek, A. Burr, N. Czink, M. Debbah, V. Degli-Esposti, H. Hofstetter, P. Kyösti, D. Laurenson, G. Matz *et al.*, "Survey of channel and radio propagation models for wireless MIMO systems," *EURASIP Journal on Wireless Communications and Networking*, vol. 2007, no. 1, pp. 56–56, 2007.

[25] T. S. Rappaport *et al.*, *Wireless communications: principles and practice*. Prentice Hall PTR New Jersey, 1996, vol. 2.

[26] T. L. Fulghum, K. J. Molnar, and A. Duel-Hallen, "The Jakes fading model for antenna arrays incorporating azimuth spread," *Vehicular Technology, IEEE Transactions on*, vol. 51, no. 5, pp. 968–977, 2002.

[27] Y. R. Zheng and C. Xiao, "Simulation models with correct statistical properties for Rayleigh fading channels," *Communications, IEEE Transactions on*, vol. 51, no. 6, pp. 920–928, 2003.

[28] F. Fuschini, E. M. Vitucci, M. Barbiroli, G. Falciasecca, and V. Degli-Esposti, "Ray tracing propagation modeling for future small-cell and indoor applications: A review of current techniques," *Radio Science*, vol. 50, no. 6, pp. 469–485, 2015.

[29] C.-X. Wang, X. Hong, H. Wu, and W. Xu, "Spatial-temporal correlation properties of the 3GPP spatial channel model and the kronecker MIMO channel model," *EURASIP Journal on Wireless Communications and Networking*, vol. 2007, no. 1, pp. 59–59, 2007.

[30] J. P. Kermoal, L. Schumacher, K. I. Pedersen, P. E. Mogensen, and F. Frederiksen, "A stochastic MIMO radio channel model with experimental validation," *Selected Areas in Communications, IEEE Journal on*, vol. 20, no. 6, pp. 1211–1226, 2002.

[31] P. Kyösti, J. Meinilä, L. Hentilä, X. Zhao, T. Jämsä, C. Schneider, M. Narandzić, M. Milojević, A. Hong, J. Ylitalo *et al.*, "WINNER II channel models," *Online: https://www.ist-winner.org/phase_2_model.html*, 2008.

[32] W. Fan, T. Jamsa, J. O. Nielsen, and G. F. Pedersen, "On angular sampling methods for 3-d spatial channel models," *Antennas and Wireless Propagation Letters, IEEE*, vol. 14, pp. 531–534, 2015.

[33] X. Cheng, C.-X. Wang, H. Wang, X. Gao, X.-H. You, D. Yuan, B. Ai, Q. Huo, L.-Y. Song, and B.-L. Jiao, "Cooperative mimo channel modeling and multi-link spatial correlation properties," *Selected Areas in Communications, IEEE Journal on*, vol. 30, no. 2, pp. 388–396, 2012.

[34] E. Dahlman, S. Parkvall, and J. Skold, *4G: LTE/LTE-Advanced for Mobile Broadband*. Amsterdam ; Boston: Elsevier/Academic Press, 2011.

[35] L. Juho, H. Jin-Kyu *et al.*, "MIMO technologies in 3GPP LTE and LTE-advanced," *EURASIP Journal on Wireless Communications and Networking*, vol. 2009, 2009.

[36] W. Chen and S. Jin, "Performance Evaluation of Closed Loop Transmission for LTE-A Uplink MIMO," in *Wireless Communications, Networking and Mobile Computing (WiCOM), 2011 7th International Conference on*, Sept 2011, pp. 1–4.

[37] E. Tuomaala and H. Wang, "Effective SINR approach of link to system mapping in OFDM/multi-carrier mobile network," in *Mobile Technology, Applications and Systems, 2005 2nd International Conference on*. IEEE, 2005, pp. 5–pp.

[38] R. Giuliano and F. Mazzenga, "Exponential effective SINR approximations for OFDM/OFDMA-based cellular system planning," *Wireless Communications, IEEE Transactions on*, vol. 8, no. 9, pp. 4434–4439, 2009.

[39] A. M. Cipriano, R. Visoz, and T. Salzer, "Calibration issues of PHY layer abstractions for wireless broadband systems," in *Vehicular Technology Conference, 2008. VTC 2008-Fall. IEEE 68th*. IEEE, 2008, pp. 1–5.

[40] E. Telatar, "Capacity of Multi-antenna Gaussian Channels," *European transactions on telecommunications*, vol. 10, no. 6, pp. 585–595, 1999.

[41] S. Schwarz, M. Wrulich, and M. Rupp, "Mutual information based calculation of the precoding matrix indicator for 3GPP UMTS/LTE," in *Smart Antennas (WSA), 2010 International ITG Workshop on*. IEEE, 2010, pp. 52–58.

[42] S. Schwarz, C. Mehlfuhrer, and M. Rupp, "Calculation of the spatial preprocessing and link adaption feedback for 3GPP UMTS/LTE," in *Wireless Advanced (WiAD), 2010 6th Conference on*. IEEE, 2010, pp. 1–6.

[43] A. J. Tenenbaum, R. S. Adve, and Y.-S. Yuk, "Channel prediction and feedback in multiuser broadcast channels," in *Information Theory, 2009. CWIT 2009. 11th Canadian Workshop on*. IEEE, 2009, pp. 67–70.

[44] K. T. Truong and R. W. Heath, "Effects of channel aging in massive MIMO systems," *Communications and Networks, Journal of*, vol. 15, no. 4, pp. 338–351, 2013.

[45] G. Caire, N. Jindal, M. Kobayashi, and N. Ravindran, "Multiuser MIMO Achievable Rates With Downlink Training and Channel State Feedback," *Information Theory, IEEE Transactions on*, vol. 56, no. 6, pp. 2845–2866, June 2010.

[46] C. Shin, R. Heath, and E. Powers, "Blind Channel Estimation for MIMO-OFDM Systems," *Vehicular Technology, IEEE Transactions on*, vol. 56, no. 2, pp. 670–685, March 2007.

[47] Y. Zeng and T.-S. Ng, "A semi-blind channel estimation method for multiuser multiantenna OFDM systems," *Signal Processing, IEEE Transactions on*, vol. 52, no. 5, pp. 1419–1429, 2004.

[48] S. Coleri, M. Ergen, A. Puri, and A. Bahai, "Channel estimation techniques based on pilot arrangement in OFDM systems," *Broadcasting, IEEE Transactions on*, vol. 48, no. 3, pp. 223–229, 2002.

[49] P. K. Pradhan, S. K. Patra, O. Faust, and B. K. Chua, "Channel estimation algorithms for OFDM systems," *International Journal of Signal and Imaging Systems Engineering*, vol. 5, no. 4, pp. 267–273, 2012.

[50] M. Meidlinger, M. Simko, Q. Wang, and M. Rupp, "Channel estimators for LTE-A downlink fast fading channels," in *Smart Antennas (WSA), 2013 17th International ITG Workshop on*. VDE, 2013, pp. 1–5.

[51] H. Hafez, Y. A. Fahmy, and M. M. Khairy, "LTE and WiMAX: performance and complexity comparison for possible channel estimation techniques," *International Journal of Communication Systems*, vol. 26, no. 6, pp. 792–805, 2013.

[52] S. Colieri, M. Ergen, A. Puri, and A. Bahai, "A study of channel estimation in OFDM systems," in *Vehicular Technology Conference, 2002. Proceedings. VTC 2002-Fall. 2002 IEEE 56th*, vol. 2. IEEE, 2002, pp. 894–898.

[53] C. Mehlführer and M. Rupp, "A robust MMSE equalizer for MIMO enhanced HSDPA," in *Signals, Systems and Computers, 2006. ACSSC'06. Fortieth Asilomar Conference on*. IEEE, 2006, pp. 129–133.

[54] C. Mehlführer, S. Caban, and M. Rupp, "An accurate and low complex channel estimator for OFDM WiMAX," in *Communications, Control and Signal Processing, 2008. ISCCSP 2008. 3rd International Symposium on*. IEEE, 2008, pp. 922–926.

[55] J. Ketonen, M. Juntti, J. Ylioinas, and J. R. Cavallaro, "Decision-directed channel estimation implementation for spectral efficiency improvement in mobile MIMO-OFDM," *Journal of Signal Processing Systems*, pp. 1–13, 2013.

[56] R. A. Akl, S. Valentin, G. Wunder, and S. Stanczak, "Compensating for CQI aging by channel prediction: The LTE downlink," in *Global Communications Conference (GLOBECOM), 2012 IEEE*. IEEE, 2012, pp. 4821–4827.

[57] K. Manolakis, S. Jaeckel, V. Jungnickel, and V. Braun, "Channel prediction by doppler-delay analysis and benefits for base station cooperation," in *Vehicular Technology Conference (VTC Spring), 2013 IEEE 77th*. IEEE, 2013, pp. 1–6.

[58] H. Shirani-Mehr, D. N. Liu, and G. Caire, "Channel state prediction, feedback and scheduling for a multiuser MIMO-OFDM downlink," in *Signals, Systems and Computers, 2008 42nd Asilomar Conference on*. IEEE, 2008, pp. 136–140.

[59] S. Semmelrodt and R. Kattenbach, "Investigation of different fading forecast schemes for flat fading radio channels," in *Vehicular Technology Conference, 2003. VTC 2003-Fall. 2003 IEEE 58th*, vol. 1. IEEE, 2003, pp. 149–153.

[60] M. Chen, M. Viberg *et al.*, "New approaches for channel prediction based on sinusoidal modeling," *EURASIP Journal on Advances in Signal Processing*, vol. 2007, 2006.

[61] K. E. Baddour and N. C. Beaulieu, "Autoregressive modeling for fading channel simulation," *Wireless Communications, IEEE Transactions on*, vol. 4, no. 4, pp. 1650–1662, 2005.

[62] B. Cheng, "Yule–Walker Equations," *Wiley StatsRef: Statistics Reference Online*, 2005.

[63] S. S. Haykin, *Adaptive filter theory*. Pearson Education India, 2007.

[64] D. Schafhuber and G. Matz, "MMSE and adaptive prediction of time-varying channels for OFDM systems," *Wireless Communications, IEEE Transactions on*, vol. 4, no. 2, pp. 593–602, 2005.

[65] M. Münster and L. Hanzo, "MMSE channel prediction assisted symbol-by-symbol adaptive OFDM," in *Communications, 2002. ICC 2002. IEEE International Conference on*, vol. 1. IEEE, 2002, pp. 416–420.

[66] I. C. Wong, A. Forenza, R. W. Heath, and B. L. Evans, "Long range channel prediction for adaptive OFDM systems," in *Signals, Systems and Computers, 2004. Conference Record of the Thirty-Eighth Asilomar Conference on*, vol. 1. IEEE, 2004, pp. 732–736.

[67] K. J. Kim, M.-O. Pun, and R. A. Iltis, "Channel prediction for limited feedback precoded MIMO-OFDM systems over time-varying fading channels," in *Information Sciences and Systems, 2008. CISS 2008. 42nd Annual Conference on*. IEEE, 2008, pp. 972–977.

[68] L. Zhang, Z. Jin, W. Chen, and X. Zhang, "An improved adaptive channel prediction for MIMO-OFDM systems," in *Communications and Networking in China, 2008. ChinaCom 2008. Third International Conference on*. IEEE, 2008, pp. 1008–1012.

[69] C. Min, N. Chang, J. Cha, and J. Kang, "MIMO-OFDM downlink channel prediction for IEEE802. 16e systems using Kalman filter," in *Wireless Communications and Networking Conference, 2007. WCNC 2007. IEEE*. IEEE, 2007, pp. 942–946.

[70] I. C. Wong and B. L. Evans, "Exploiting Spatio-Temporal Correlations in MIMO Wireless Channel Prediction," in *Global Telecommunications Conference, 2006. GLOBECOM'06. IEEE*. IEEE, 2006, pp. 1–5.

[71] L. Liu, H. Feng, T. Yang, and B. Hu, "MIMO-OFDM Wireless Channel Prediction by Exploiting Spatial-Temporal Correlation," *Wireless Communications, IEEE Transactions on*, vol. 13, no. 1, pp. 310–319, 2014.

[72] H. Senol, H. A. Çirpan, E. Panayírcí, and M. Çevik, "A low-complexity time-domain MMSE channel estimator for space-time/frequency block-coded OFDM systems," *EURASIP Journal on Applied Signal Processing*, vol. 2006, pp. 242–242, 2006.

[73] S. Galih, R. Karlina, F. Nugroho, A. Irawan, T. Adiono, and A. Kurniawan, "Low complexity down-sampled MMSE (DMMSE) channel estimation for downlink OFDMA IEEE 802.16 e system," in *2009 3rd IEEE International Symposium on Microwave, Antenna, Propagation and EMC Technologies for Wireless Communications*, 2009.

[74] M. Simko, C. Mehlfuhrer, M. Wrulich, and M. Rupp, "Doubly dispersive channel estimation with scalable complexity," in *Smart Antennas (WSA), 2010 International ITG Workshop on*, Feb 2010, pp. 251–256.

[75] L. Yong-Hwan, "Complexity-reduced channel estimation in spatially correlated MIMO-OFDM systems," *IEICE transactions on communications*, vol. 90, no. 9, pp. 2609–2612, 2007.

[76] I. C. Wong and B. L. Evans, "Joint channel estimation and prediction for OFDM systems," in *Global Telecommunications Conference, 2005. GLOBECOM'05. IEEE*, vol. 4. IEEE, 2005, pp. 5–pp.

[77] P. Suárez-Casal, J. A. García-Naya, L. Castedo, and M. Rupp, "Channel Estimation in Spatially Correlated High Mobility MIMO-OFDM Systems," in *Wireless Communication Systems (ISWCS 2013), Proceedings of the Tenth International Symposium on*. VDE, 2013, pp. 1–5.

[78] S.-K. Kim and Y.-H. Lee, "3-dimensional MMSE channel estimation in multi-antenna OFDM systems," in *Digital Telecommunications, 2008. ICDT'08. The Third International Conference on*. IEEE, 2008, pp. 6–10.

[79] R. O. Adeogun, P. D. Teal, and P. A. Dmochowski, "Parametric Channel Prediction for Narrowband Mobile MIMO Systems Using Spatio-Temporal Correlation Analysis," in *Vehicular Technology Conference (VTC Fall), 2013 IEEE 78th*. IEEE, 2013, pp. 1–5.

[80] D. Sun, Z. Liu, S. Ma, and K. Yi, "Channel Prediction Using IAA-Based Spectral Estimation in Precoded TDD-MIMO Systems," *Communications Letters, IEEE*, vol. 17, no. 4, pp. 701–704, April 2013.

[81] A. Duel-Hallen, "Fading Channel Prediction for Mobile Radio Adaptive Transmission Systems," *Proceedings of the IEEE*, vol. 95, no. 12, pp. 2299–2313, Dec 2007.

[82] W. Yang, G. Durisi, and E. Riegler, "On the capacity of large-mimo block-fading channels," *Selected Areas in Communications, IEEE Journal on*, vol. 31, no. 2, pp. 117–132, 2013.

[83] A. Ancora, C. Bona, and D. T. Slock, "Down-sampled impulse response least-squares channel estimation for LTE OFDMA," in *Acoustics, Speech and Signal Processing, 2007. ICASSP 2007. IEEE International Conference on*, vol. 3. IEEE, 2007, pp. III–293.

[84] Y. Xia, T. Chen, and J. Shan, "A novel iterative method for computing generalized inverse," *Neural computation*, vol. 26, no. 2, pp. 449–465, 2014.

[85] Y. Li and L. Cimini, "Bounds on the interchannel interference of OFDM in time-varying impairments," *Communications, IEEE Transactions on*, vol. 49, no. 3, pp. 401–404, Mar 2001.

[86] A. F. Molisch, M. Toeltsch, and S. Vermani, "Iterative methods for cancellation of intercarrier interference in OFDM systems," *Vehicular Technology, IEEE Transactions on*, vol. 56, no. 4, pp. 2158–2167, 2007.

[87] J. P. Patra and P. Singh, "Joint iterative CCI and ICI cancellation for STBC-OFDM system in fast fading channel," in *Computer and Communication Technology (ICCCT), 2014 International Conference on*. IEEE, 2014, pp. 205–210.

[88] N. Keita, K. Nishimori, S. Sasaki, and H. Makino, "Spatial multiplexing for multiple users exceeding degree of freedom by successive interference cancellation and zero forcing," in *Electromagnetics (iWEM), 2014 IEEE International Workshop on*. IEEE, 2014, pp. 94–95.

[89] G. Tauböck, M. Hampejs, G. Matz, F. Hlawatsch, K. Gröchenig *et al.*, "Low-complexity ICI/ISI equalization in doubly dispersive multicarrier systems using a decision-feedback LSQR algorithm," *Signal Processing, IEEE Transactions on*, vol. 59, no. 5, pp. 2432–2436, 2011.

[90] H. Zarrinkoub, *Understanding LTE with MATLAB : from mathematical foundation to simulation, performance evaluation and implementation*. John Wiley & Sons, Ltd, 2014.

[91] L. Hentilä, P. Kyösti, M. Käske, M. Narandzic, and M. Alatossava, "MATLAB implementation of the WINNER Phase II Channel Model ver1. 1," *Online: https://www.ist-winner.org/phase_2_model.html*, 2007.

[92] P. E. Black, "Big-o notation," *Dictionary of Algorithms and Data Structures*, vol. 2007, 2007.

APPENDIX A

PUBLICATIONS

- **Conference Proceedings**

  Gichohi Karuga, Edward Ndungu, Kibet Langat, "Low Complexity MMSE Channel Prediction for Block Fading Channels in LTE Downlink," *Proceedings of the 12th IEEE AFRICON International Conference*, 14-17 Sept. 2015, pp.57-61. http://ieeexplore.ieee.org/xpl/articleDetails.jsp?arnumber=7331981

- **Journal**

  Gichohi Karuga, Edward Ndungu, Kibet Langat, "3D Channel Prediction for Doubly Dispersive Channels in LTE Downlink," *Journal of Sustainable Research in Engineering* Vol. 2 (3) 2015, 76-83.
  http://www.jkuat-sri.com/ojs/index.php/sri/article/view/354